

Long-Term Changes of Greenhouse Gases in the Ocean and Their Feedback Effects on the Climate

Yutaka W. Watanabe^{1*}, Ichiro Yasuda² and Nobuo Tsurushima³

¹Faculty of Earth Environmental Science, Hokkaido University, Japan

²Atmosphere and Ocean Research Institute, The University of Tokyo, Japan

³National Institute of Advanced Industrial Science and Technology, Japan

*E-mail: yywata@ees.hokudai.ac.jp

Keywords: Decadal Climate Change; Greenhouse Gases

Introduction

Based on models and observations, a decrease in water formation rate has already been caused in a response to global warming (e.g., Levitus *et al.* 2001). Recent hydrographic data have also shown that the oceanic biogeochemical conditions have changed on a decadal scale (e.g., Karl *et al.* 2001). The most important key areas for biogeochemical changes are the intermediate-deep water formation areas, especially, the high latitudinal productive areas such as the North Atlantic, the Southern Oceans, and the North Pacific subpolar region. Clarification of what causes the long-term changes of oceanic physical and biogeochemical conditions is an essential step for predicting global climate changes in the future.

The North Pacific subpolar region has a relatively high primary productivity compared with the subtropical regions, which arises from larger-sized phytoplankton such as diatoms (e.g., Honda *et al.* 2002). Consequently, this region is an important sink of CO₂ (e.g., Takahashi *et al.* 2002). Recent studies have already reported linear increases of temperature (T) and phosphate (PO₄), and linear decreases of salin-

ity (S) and dissolved oxygen (DO), in the western and eastern sides of the North Pacific (e.g., Watanabe *et al.* 2003), which were superimposed on decadal oscillation. However, each study was based only on a time series of a local fixed observation point, and/or the composite of different qualitative data sets with large systematic errors. Thus, it is difficult to comprehend quantitatively all the biogeochemical changes throughout the entire polar/subpolar region, and to clarify the consequent factors causing a biogeochemical impact such as the imbalance of nitrogen and/or carbon in the ocean. The integrative analysis derived from a time series of several fixed observation points is necessary. Here we have focused on several time series data sets covering the North Pacific region, and have tried to integrate them in order to clarify the possibility of biogeochemical change such as a shift of biological species.

In addition, according to these biogeophysical decadal changes in the North Pacific, it is important to clarify whether the feedback systems to the climate changes work or not. Therefore, we tried to construct a spatiotemporal algorithm of several properties as feedback

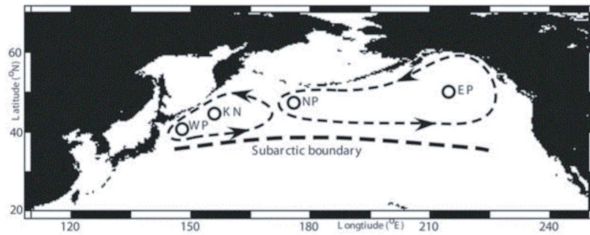


Fig. 1. Map for the North Pacific subpolar region showing the positions of time series data of hydrographic properties used in this study. The symbols ‘EP’, ‘NP’, ‘KN’ and ‘WP’ are the hydrographic observation sites. The schematic sea surface currents are also shown based on Ohtani (1991).

parameters based on the observational multiple parameters in the North Pacific, and to reconstruct their long-term change in the North Pacific subpolar and subtropical regions during the last several decades. Furthermore, we have sought to make model simulations to reconstruct the climate changes of physical and biogeochemical properties in the North Pacific. In the following sections, we will show some remarkable results of our study.

Evidence of Changes in Oceanic Biogeochemical Parameters with Decadal Climate Change in the North Pacific

Here, we have focused on four time series data sets of fixed observation sites covering the North Pacific region, and tried to integrate them in order to clarify the possibility of biogeochemical change such as a shift of biological species.

Data and methods

We used the following four time series data sets of biogeochemical properties within two representative gyres of the North Pacific (Ohtani 1991) (Fig. 1). At Station Western Pacific (Sta. WP: 42°N, 144–147°N), the Hakodate Marine Observatory of Japan Meteorological Agency has conducted hydrographic observations 4–5 times a year in the Oyashio region

from 1968 to the present (JMA 2001). Time series observations at Station KNOT (Sta. KN: 44°N, 155°E) has been carried out from 1998 to the present (JODC 2004), and at Station NOPACCS/WESTCOSMIC (Sta. NP: 48°N, 175°E) observations have been made from 1991 to 2001 as part of NOPACCS and WEST-COSMIC (KANSO 2006). At Station Eastern Pacific (Sta. EP: 50°N, 145°W), the Institute of Ocean Sciences has carried out the hydrographic observations several times a year from 1956 to the present (Institute of Ocean Sciences 2006). All the DO and nutrients were measured by the Winkler method, the molybdenum photometric method and the copper-cadmium sulfanilamide reduction method, as classical methods. An offset between the entire cruises had been estimated to be less than $0.1 \mu\text{mol kg}^{-1}$ for PO_4 , $1 \mu\text{mol kg}^{-1}$ for $\text{NO}_2 + \text{NO}_3$, $5 \mu\text{mol kg}^{-1}$ for Si, and $5 \mu\text{mol kg}^{-1}$ for DO, respectively. We used these data here without any correction for the offsets in this study. Using PO_4 and $\text{NO}_2 + \text{NO}_3$, we also estimated N^* ($=[\text{NO}_2 + \text{NO}_3] - R_{\text{NP}} \cdot (\text{PO}_4) + 2.9$, where $R_{\text{NP}} = 16$ (Deutsch *et al.* 2001)) as an index of nitrogen fixation-denitrification.

Both Stas. KN and NP did not have sufficient decadal time series individually. Since the structure of the surface water mass in the North Pacific subpolar region mainly consists of the Western Subarctic

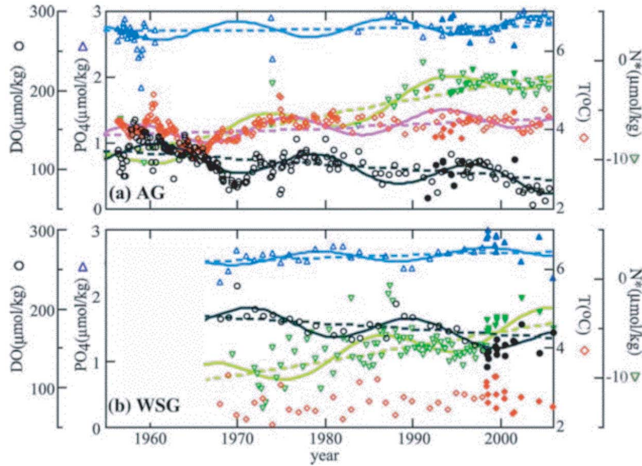


Fig. 2. Time series of DO (black circle), PO₄ (blue triangle), T (red diamond) and N* (green triangle) in the subsurface water. Open symbols are Stas. EP and WP, and solid ones are Stas. NP and KN. Solid and dashed lines indicate the significant fitted curves and linear trends. (a) Time series on $26.8\sigma_{\theta}$ within AG. (b) Time series on $26.8\sigma_{\theta}$ within WSG.

Gyre (WSG) and the Alaskan Gyre (AG) (Ohtani 1991), we considered that both Stas. KN and WP are located within WSG, and both Stas. NP and EP are within AG. In previous studies, many hydrographic properties have shown a long-term linear trends and oscillations (e.g., Watanabe *et al.* 2003). Therefore, in order to distinguish between them, we have applied an equation of the Fourier sine expansion to the time series data sets of each site: ($X = -a \cdot y + b + c \cdot \sin\{2\pi(y - d)/e\}$), where 'X' refers to one of several properties. 'y' is the calendar year. 'a'-'e' are constants. That is, $X = \text{linear trend component (L)} + \text{oscillation component (O)}$.

Results

Over this region, we found significant linear trends of hydrographic properties that were superimposed on the decadal periodicity. For DO, PO₄, T and N* on $26.8\sigma_{\theta}$ below the winter mixed layer (Fig. 2), the trends and oscillations in the two gyres were almost the same while there were opposite phases of oscillation between the two gyres. As the averaged trend

and oscillation in the two gyres, DO_{ave} was $-0.74 \pm 0.01 \mu\text{mol kg}^{-1} \text{y}^{-1}$ and $17.6 \pm 0.4 \text{y}$; $\text{PO}_{4\text{ave}}$ was $+0.003 \pm 0.001 \mu\text{mol kg}^{-1} \text{y}^{-1}$ and $18.1 \pm 1.4 \text{y}$; T_{ave} was $+0.003 \pm 0.002^{\circ}\text{C y}^{-1}$ and 17.6y ($n = 1$); N^*_{ave} was $+0.18 \pm 0.00 \mu\text{mol kg}^{-1} \text{y}^{-1}$ and $19.9 \pm 1.1 \text{y}$.

On the other hand, in the surface mixed layer in springtime (April–June) (Fig. 3), the trends and oscillations of σ_{θ} , S and Si in both gyres were also almost the same with the opposite phases between the two gyres. However, the trends of NO₂ + NO₃ and N* in the east were more than twice as that in the west. As the averaged trend and oscillation, $\sigma_{\theta\text{ave}}$ was $-0.006 \pm 0.000 \text{y}^{-1}$ and not significant (ns); Si_{ave} was $-0.20 \pm 0.01 \mu\text{mol kg}^{-1} \text{y}^{-1}$ and ns; S_{ave} was $-0.001 \pm 0.001 \text{y}^{-1}$ and 19.3y ($n = 1$); NO₂ + NO₃ ave was $-0.10 \mu\text{mol kg}^{-1} \text{y}^{-1}$ ($n = 1$) and ns; N^*_{ave} was $+0.12 \pm 0.06 \mu\text{mol kg}^{-1} \text{y}^{-1}$ and $18.9 \pm 1.3 \text{y}$.

Discussion

(1) Changes of biogeochemical properties in the subsurface water

The water mass centered on $26.8\sigma_{\theta}$ is

Table 1. The linear trend (L) and Oscillation (O) of hydrographic parameters in the North Pacific subpolar region*.

	WSG		AG	
	L	O	L	O
	⟨Subsurface:26.8 σ_θ ⟩			
DO, $\mu\text{mol kg y}^{-1}$	-0.73 ($p < 0.001$)	18.3y ($r = 0.83$)	-0.75 ($p < 0.0001$)	17.9y ($r = 0.78$)
PO ₄ , $\mu\text{mol kg y}^{-1}$	+0.003 ($p < 0.10$)	19.1y ($r = 0.60$)	+0.002 ($p < 0.01$)	17.1y ($r = 0.56$)
T, $^\circ\text{C y}^{-1}$	ns	ns	+0.011 ($p < 0.001$)	17.6y ($r = 0.73$)
N*, $\mu\text{mol kg y}^{-1}$	+0.18 ($p < 0.001$)	19.1y ($r = 0.55$)	+0.18 ($p < 0.005$)	20.7y ($r = 0.87$)
	⟨Surface⟩			
σ_θ , y^{-1}	-0.006 ($p < 0.05$)	ns	-0.006 ($p < 0.005$)	ns
Salinity, y^{-1}	-0.004 ($p < 0.10$)	ns	-0.002 ($p < 0.001$)	19.3y ($r = 0.60$)
Si, $\mu\text{mol kg y}^{-1}$	-0.19 ($p < 0.05$)	ns	-0.21 ($p < 0.001$)	ns
NO ₂ + NO ₃ , $\mu\text{mol kg y}^{-1}$	ns	ns	-0.10 ($p < 0.05$)	ns
N*, $\mu\text{mol kg y}^{-1}$	+0.07 ($p < 0.01$)	18.0y ($r = 0.50$)	+0.15 ($p < 0.001$)	19.8y ($r = 0.85$)

*Here ns: not significant; p : the coefficient at a 95% confidence level for the linear trend; r : the correlation coefficient for the fitted curve equation.

the North Pacific Intermediate Water (NPIW) which is the only water mass produced in the North Pacific subpolar region, and it spreads over the North Pacific. The origin is near the transition domain east off Japan and the Sea of Okhotsk. NPIW flows almost directly eastward, taking 5 to 7 years to reach Sta. EP in AG (Ueno and Yasuda 2003). Yasuda *et al.* (2006) showed a possibility that an 18.6-year period nodal tidal cycle links to decadal variations of hydrographic properties. Andreev and Baturina (2006) also found that a decadal change of DO in NPIW could be described by a combination of the intensity of the Aleutian Low pressure, the wind stress and the tidal amplitude. Thus, these mechanisms and the eastward transported time of NPIW may result in the oscillation of 18 years in these properties and its opposite phase in the two gyres.

On the other hand, it is possible that the trend has been caused by a reduction in formation of NPIW due to global warming, which has already been supported by several recent reports (e.g., Emerson *et al.* 2004). However, it is difficult to explain the same trend between the two gyres based on only the circulation of NPIW. NPIW is diluted by 50% with ambient water from WSG to AG (e.g., Watanabe *et al.* 1995; Whitney *et al.* 2007). If the ori-

gin of the changes of hydrographic properties in NPIW is only in WSG, the intensity of the trend of each property in AG will be about half as that in WSG. However, the actual trend was almost the same between the two gyres. For example, the trend of DO of $-0.75 \mu\text{mol kg}^{-1} \text{y}^{-1}$ in WSG closely agreed with those of $-0.73 \mu\text{mol kg}^{-1} \text{y}^{-1}$ in AG. Therefore, it is possible that the intensity of other factors causing the trend is equivalent to the intensity of circulation of NPIW because all the properties' trends are almost the same between the two gyres despite a mixing of 50%. Apart from the circulation of NPIW, what mainly causes the trends of hydrographic properties over the subpolar region?

(2) Implications of linear increasing trend of N*

The time series of hydrographic properties in the surface mixed layer in spring-time could help to clarify the cause of the trend (Fig. 3). The surface density (σ_θ) has declined with a decrease of salinity in the two gyres, indicating the progression of stratification of surface mixed layer in the past five decades. With the reinforcement of stratification, Si also decreased by $0.2 \mu\text{mol kg}^{-1} \text{y}^{-1}$ in both gyres. NO₂ + NO₃ in AG has decreased while that in WSG has not changed significantly. Furthermore, the

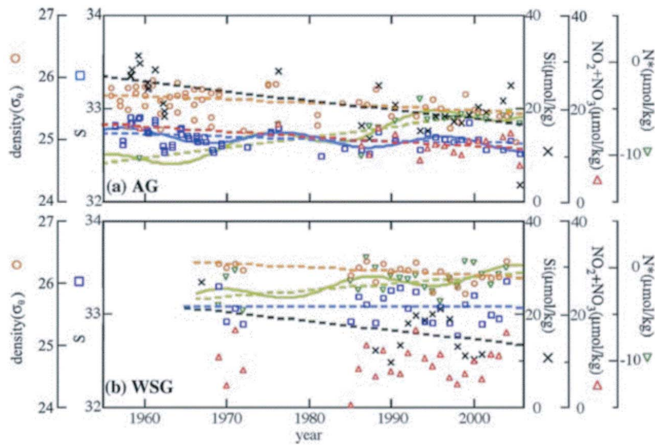


Fig. 3. Time series of σ_θ (orange circle), S (blue square), Si (black cross), $\text{NO}_2 + \text{NO}_3$ (red triangle) and N^* (green triangle) in the surface mixed layer in the springtime. We used average values within the surface mixed layer. Solid and dashed lines indicate the significant fitted curves and linear trends. (a) Time series within AG. (b) Time series within WSG.

Si/N ratio has decreased from 2.1 ± 0.3 to 1.4 ± 0.1 during the past five decades. N^* has increased by $0.07\text{--}0.16 \mu\text{mol kg}^{-1} \text{y}^{-1}$ as well as that in NPIW, and the trend of N^* in the east was twice that in the west.

In order to explain the same trend between the two gyres apart from the circulation of NPIW, we here focus on the change of N^* and consider the following four possibilities: (i) the increase of supply of higher N^* from intermediate/deep to surface waters; (ii) the increase of input of N from rivers and/or atmosphere; (iii) the increase of diazotrophs; and (iv) the decrease of the N/P ratio required for diatoms as a consequence of iron deficiency.

Yamagishi *et al.* (2005) reported the denitrification in DO minimum zone of NPIW. Regarding the possibility of (i), because DO has declined during the past five decades in NPIW in both gyres (Fig. 2), it is difficult to cause the increase of N^* by a decrease of denitrification through the water column. The increase of N^* may be mainly caused by a decrease of denitrification in the original area of NPIW near the transition domain in WSG. How-

ever, a recent re-observation near the Sea of Okhotsk in WSG showed a remarkable decrease of N^* in the past decade, which was due to the reinforcement of denitrification arising from a change of bacterial activity (Watanabe and Nishioka 2007). Furthermore, considering that the increasing trend of N^* in NPIW is the same in both gyres, and that the mixing of 50% occurs eastward, a weakness of denitrification only around WSG can not explain the increase of N^* in the two gyres.

In the case of (ii), the Amur River and/or Asian dust may play an important role in causing the increase of N^* over this region. Since both these sources are located at the westernmost side, the influence of these changes generally decreases eastward (e.g., Mahowald *et al.* 2005), which can not explain the same trend of N^* in NPIW in both gyres and the larger trend of N^* in the surface of AG. There was no actual remarkable decrease of salinity causing an increase of N in the surface, indicating that the influence of river was at the most small. Furthermore, it would be also difficult for the changes of the

Amur River and Asian dust simultaneously to cause the opposite phases of oscillation of N^* between the two gyres.

Regarding the possibility of (iii), using model calculation based on the residual of PO_4 under conditions when nitrogen was deficient, Deutsch *et al.* (2007) suggested a possibility of the existence of diazotrophs in the North Pacific subpolar region although the ratio of diazotrophs to the export flux was less than 10%. In general, PO_4 remains when N is deficient in the surface water of the subpolar region. However, we can not know whether diazotrophs have recently increased or not in this region since their abundance is small. Therefore, the possibility of (iii) may be small although it is not possible to rule it out without further data.

Consequently, the possibility of (iv) as a decrease of the N/P ratio required for diatoms as a consequence of iron deficiency could possibly result in the trend of N^* in this region. Price (2005) reported that the ratio of N/P of diatoms declines by two thirds under iron-limited conditions. In addition, several reports showed that the ratio of Si/N of diatoms increases by a factor of 2–3 under iron-limited conditions (e.g., Hutchins and Bruland 1998). According to these studies, when the sea surface water within a domain of diatoms continues to exist under iron-deficient conditions, N^* must increase with decreasing Si. On the other hand, the primary production generally decreases under iron-limited condition. Maldonado *et al.* (2001) has shown that diatom sinking rates are faster by a factor of four under iron-limited condition than iron-replete condition, which implies that a greater fraction of the primary production may be exported even though the total amount of primary production would decline. This enables us to explain the decrease of DO in NPIW with increasing N^* in the surface.

N^* has actually increased with decreasing Si in the surface water, and the surface

mixed layer in AG has about twice the increasing trend of N^* as in WSG. Suzuki *et al.* (2002) reported that the limitations of iron and nitrogen in AG were larger than those in WSG. If the mixing of NPIW occurs by 50% eastward, the intensity of decrease of N/P of diatoms in AG can explain most of the causes for the same trend of N^* between the two gyres. Consequently, we can find that the trends of N^* in both gyres were the same, despite the eastward mixing, suggesting the probability of recent reduction of iron supplied from deep water to surface water, and a probability of a shift of phytoplankton including the physiological and/or phytoplankton community structure changes with the decrease of primary productivity as a result of the reinforcement of stratification. However, the possibility of (iv) alone can not completely explain the increasing trend of N^* in NPIW because a part of lower N/P organic matter by diatom is regenerated in the subsurface, which suggests that there has been already a possibility of the case of (iii) in addition to the case of (iv). Therefore, the decadal increase of N^* must be caused by a combination of the change of formation of NPIW, the decrease of N/P of nutrient uptake by diatoms, and/or the increase of diazotrophs.

In the surface mixed layer, if Si continues to decline at the current trend of $-0.2 \mu\text{mol kg}^{-1} \text{y}^{-1}$, Si will be depleted in the next 70 years while N of $3.3 \mu\text{mol kg}^{-1}$ and P of $0.5 \mu\text{mol kg}^{-1}$ will still be retained. Furthermore, contiguous depletion of nutrient property is N while P of $0.2 \mu\text{mol kg}^{-1}$ will remain for about 30 years after the depletion of Si. Deutsch *et al.* (2007) has already suggested a possibility of the existence of diazotrophs in the subpolar region. Additionally, IPCC (2007) reported that precipitation in the subpolar region will increase by the next century. Jo *et al.* (2007) revealed that the Asian dust supplied via the precipitation is available

for the phytoplankton in the North Pacific. If the precipitation increases with a constant intensity of Asian dust, the atmospheric supply of iron to the sea surface would increase. Since N is depleted by the ocean stratification in this time, diazotrophs may appear remarkably over the subpolar region. The shift of phytoplankton in regions with high primary productivity may play an important role in the global balances of nitrogen and carbon in the future.

Reconstruction of Sea Surface Dimethylsulfide in the North Pacific during 1970s to 2000s

According to these biogeophysical decadal changes in the North Pacific, it is important to clarify whether the feedback systems to the climate changes work or not. We have tried to construct a spatiotemporal algorithm of DMS (dimethylsulfide) as negative feedback parameters based on the multiple observational parameters in the North Pacific, and to reconstruct their long-term change in the North Pacific subpolar and subtropical regions during the last several decades.

Introduction

DMS is produced by marine phytoplankton activity, and its content in the surface mixed layer is supersaturated with respect to the atmosphere. Consequently, the net flux of DMS is driven from sea to air. In the atmosphere, DMS is rapidly oxidized to form sulfur aerosols, and the cloud condensation nuclei derived from DMS acts to counter global greenhouse warming. Thus it is important to understand the spatiotemporal distribution of DMS flux for predicting future global climate change (e.g., Andreae 1990). To understand the global oceanic distribution of DMS, several attempts have been made to parameterize the global spatiotemporal distribution of sea surface DMS using oce-

anic climatological parameters (chlorophyll-a (Chl), light intensity (I), nutrients (N), surface mixed layer depth (MLD)) or using ocean models (Anderson *et al.* 2001; Simó and Dachs 2002; Aumont *et al.* 2002; Chu *et al.* 2003; Belviso *et al.* 2004b). However, Belviso *et al.* (2004a) demonstrated that there were large uncertainties and spatial differences of sea surface DMS between these studies. Especially, in the North Pacific, even the algorithm of Simó and Dachs (2002) yielding the results of being the most similar to the observational sea surface DMS, gave values under half of the observational data.

On the other hand, recent studies of global climate change have reported the possibility that recent oceanic conditions have changed due to the effect of anthropogenically induced greenhouse warming and/or natural climate change (e.g., Levitus *et al.* 2000; Hansen *et al.* 2002). In the North Pacific, some studies have already shown the changes of chemical components with the decrease of sea surface water density, suggesting a weakening of the surface-deep water mixing derived from artificial greenhouse warming effects and/or natural climate change (Ono *et al.* 2001; Watanabe *et al.* 2001, 2003; Emerson *et al.* 2004). Consequently, the abundances of phytoplankton and Chl in the surface mixed layer have been shown to decrease in the North Pacific subpolar and subtropical regions (e.g., Gregg and Conkright 2002; Chiba *et al.* 2004; Watanabe *et al.* 2005). In addition, Karl *et al.* (2001) indicated the increase of nitrogen fixing smaller-size phytoplankton in the subtropical region, and Ishida *et al.* (2009) demonstrated the possibility of a shift in the phytoplankton from a larger size of $>3 \mu\text{m}$ to a smaller size of $<3 \mu\text{m}$, suggesting the possibility a domain shift of phytoplankton from large size species to small size species as a high-producer group of DMS (e.g., Malin and Kirst 1997). According to these biogeophysical

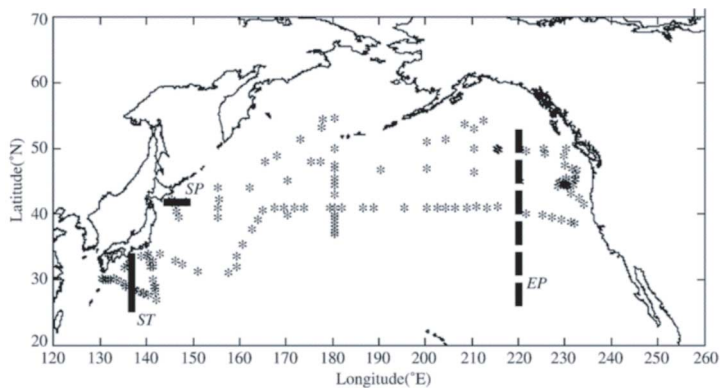


Fig. 4. Map for the North Pacific indicating the positions of data set of DMS, Chl, SST and SSN used in this study. A bold dotted line, 'EP' indicates the positions of independent DMS dataset set along 140°W from 25°N to 55°N (Bates and Quinn 1997) which were not used to construct our DMS algorithm. Bold lines, 'SP' and 'ST' are the subpolar and subtropical time series datasets of hydrographic parameters from 1971 to 2000, respectively (Japan Meteorological Agency 2001) (see Table 2).

decadal changes in the North Pacific, it is important to clarify whether the flux of oceanic DMS has changed or not. In the North Pacific, therefore, we have constructed a spatiotemporal algorithm of sea surface DMS based on the observational sea surface DMS with other hydrographic multiple parameters in the North Pacific, and to reconstruct the long-term change of sea surface DMS in the North Pacific subpolar and subtropical regions during the last several decades.

Data and method

(1) Concept for construction of DMS algorithm

As the concentration of sea surface DMS relates to the phytoplankton activity (e.g., Malin and Kirst 1997), we assumed that the concentration of DMS depends on the biological parameters relating to a growth rate of phytoplankton. That can be generally expressed by the following exponential function:

$$\text{DMS} = a \cdot B_0 \cdot \exp(f_{(\text{SST}, I, N)}), \quad (1)$$

where 'a', 'B₀', 'SST', 'I' and 'N' are the

coefficient of transformation from B₀ to DMS, the initial phytoplankton biomass, the sea surface temperature, the light intensity, and the concentration of nutrient, respectively. Until now, it was difficult to measure simultaneously both B₀ and I with DMS in the observational time. In many hydrographic observations, Chlorophyll-a (Chl) has generally been measured as an index of biological activity. It is possible that an averaged meridional pattern of I is roughly similar to that of the cosine of latitude due to the derivation of sun radiation. Most of phytoplankton activities are generally limited by nitrate or iron in the surface mixed layer (e.g., Imai *et al.* 2002). We therefore tried to use Chl, the cosine of latitude at the observational position (cos(L)) and the sea surface nitrate (SSN), as proxies of B₀, I and N, respectively:

$$\text{DMS} = a \cdot b \cdot \text{Chl} \cdot \exp(f_{(\text{SST}, \cos(L), \text{SSN})}), \quad (2)$$

where 'b' is the coefficient of transformation from B₀ to Chl.

It is actually difficult to know $f_{(\text{SST}, \cos(L), \text{SSN})}$ directly. In such a case, the multiple linear regression technique has

Table 2. A list of cruise information for DMS data set used in this study.

Cruise name	Sampling date	Sampling area	Numbers of data	References
<DMS, Chl, SSN and SST data set to construct DMS algorithm>				
KH1988	Jun.–Aug. 1988	54°N–31°N, 140°E–126°W	71	Watanabe <i>et al.</i> (1995a,b)
KH1997	Jun.–Sep. 1997	55°N–42°N, 148°E–140°W	20	Aranami <i>et al.</i> (2002)
IOS-1996–2001	May 1996–Aug. 2001	50°N–48°N, 144°W–126°W	255	Wong <i>et al.</i> (2005), IOS (2006) ^a
OS1990	Jul. 1990–Jul. 2002	54°N–37°N, 160°W–148°W	37	This study
KH1991	Jan.–Feb. 1991	27°N–30°N, 135°E–141°W	67	This study
KT1991	Jun. 1991	34°N–27°N, 133°E–142°E	40	This study
HNF2002–2003	Jun. 2002–Jun. 2003	43°N–39°N, 145°E–147°E	14	This study
<DMS data set to evaluate the validity of DMS algorithm>				
(Eastern Pacific: EP)				
Surveyor 1993	Apr.–May 1993	25°N–55°N, 140°W	163	Bates and Quinn (1997)
(Subpolar region: SP)				
HNF2004–2005	Jan. 2004–Jan. 2005	43°N–39°N, 145°E–147°E	39	This study
(Subtropical region: ST)				
KH1991	Jan.–Feb. 1991	27°N–30°N, 137°E–139°W	6	This study
KT1991	Jul. 1991	27°N–30°N, 135°E–141°W	7	This study
<Hydrographic data set to reconstruct the time series of DMS>				
(Subpolar region: SP)				
Kofu	Feb. 1971–Dec. 1998	42°N, 144°E–147°E	866	JMA(2001) ^b
(Subtropical region: ST)				
Ryofu	Jan.–Feb. Aug.–Sep. 1971–2000	34°N–25°N, 137°E	1100	JMA(2001) ^b

^aInstitute of Ocean Sciences.

^bJapan Meteorological Agency.

been generally useful to clarify the relationship between several parameters in many hydrographic researches (e.g., Sabine *et al.* 2004). Assuming that $f_{(SST, \cos(L), SSN)}$ can be expressed by a multiple linear regression, therefore, we can obtain the following equation:

$$DMS = a \cdot b \cdot Chl \cdot \exp(c \cdot SST + d \cdot \cos(L) + e \cdot SSN + f), \quad (3)$$

where ‘ c – f ’ are constants. ‘ f ’ is the intercept in the multiple linear regression. Expressing Eq. (3) as a natural logarithm form, we can obtain the following equation:

$$\begin{aligned} \ln DMS &= \ln a + \ln b + \ln Chl + c \cdot SST + d \cdot \cos(L) \\ &\quad + e \cdot SSN + f \\ &= \ln Chl + c \cdot SST + d \cdot \cos(L) + e \cdot SSN + g, \end{aligned} \quad (4)$$

where ‘ g ’ is the sum of $\ln a$, $\ln b$ and f . Substituting all the observational DMS data equipped with Chl, SST and SSN for Eq. (4) over the North Pacific, we carried out

a statistical test in order to validate the usefulness of each parameter in the multiple linear regression.

(2) Data

To construct an algorithm of sea surface DMS (nM) over the North Pacific based on Eq. (4), we used all the observational DMS data set equipped with Chl ($\mu\text{g/l}$), SST (K) and SSN (μM) from the 1980s to the 2000s over the northern North Pacific (Watanabe *et al.* 1995a, b; Aranami *et al.* 2002; Wong *et al.* 2005; IOS 2006) (our new data) (the percentage from each decade: 1980s (14%), 1990s (67%), 2000s (19%)) (Fig. 4 and Table 2). The total data set we addressed were 504 data set collected in 0–20 m depths in the region from 25°N to 55°N, including all seasons (the percentage from each period: January–March (18%), April–June (43%), July–September (36%), October–December (3%)). DMS was usually measured by the general pre-concentrated gas-chromatographic method (e.g., Watanabe *et al.* 1995b). We also used the datasets of Chl and SSN measured by the solvent extraction photofluorimetric method (Yentsch

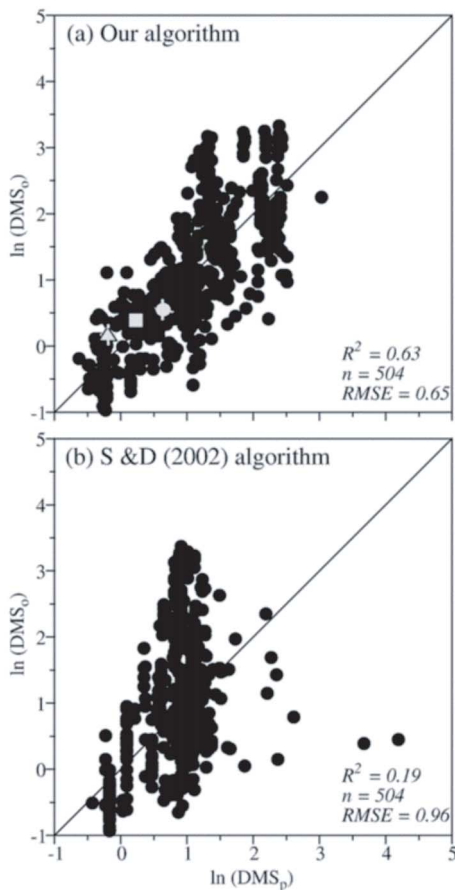


Fig. 5. Plots of the observed DMS (DMS_o , nM) versus the predicted DMS (DMS_p , nM) over the North Pacific. (a) The plot of DMS_o and DMS_p estimated from Eq. (5) in our study ($R^2 = 0.63$, $RMSE = 0.65$ (or ± 1.9 nM), $n = 504$). Solid line represents the 1:1 line between DMS_o and DMS_p . Both DMS_o and DMS_p are shown as natural logarithm values. We also showed the comparison between DMS_o and DMS_p in the EP line. Gray triangle, square and circle were the averaged value of sea surface DMS south of 30°N , that from 30°N to 40°N , and that north of 40°N , respectively. We here applied an empirical equation of SSN derived from SST and Chl (Goes *et al.* 2000) to the EP line because the EP line had no data of SSN despite being of the dataset of SST and Chl. The error bars indicate the standard errors of averaged values (SE). (b) Same as panel (a), but calculated from the algorithm of Simó and Dachs (2002) ($R^2 = 0.19$, $RMSE = 0.96$ (or ± 2.6 nM), $n = 504$). The algorithm was based on the ratio of Chl and the surface mixed layer depth with a difference of $0.125 \sigma_\theta$ from the surface density (MLD, m). Thus we here used the same data set of Chl as used to construct our DMS algorithm. In these hydrographic data positions, we calculated the monthly MLD based on climatological temperature and salinity data from World Ocean Atlas 2001 (Stephens *et al.* 2002; Boyer *et al.* 2002). Applying the above Chl and MLD into their algorithm, we obtained the relationship between DMS_o and DMS_p .

and Menzel 1963), and the copper-cadmium sulfanilamide reduction method (Strickland and Parsons 1968). The precisions of DMS, SSN and Chl were estimated to be approximately $\pm 6\%$, $\pm 2\%$ and $\pm 10\%$, respectively, which were obtained from duplicate determinations in the surface water.

Results and discussion

(1) Parameterization of sea surface DMS over the North Pacific

In general, the F -test is used to validate the usefulness of each parameter in the multiple linear regression. In our study, the parameter with F value greater than 2.4 has a significant meaning (e.g., Wilks 1995), indicating that it is useful to obtain an empirical equation in the multiple linear regression. By using a stepwise linear fitting regression for Eq. (4) with the F -test, the first term of right-hand side in Eq. (4), $\ln\text{Chl}$ was only found to become negligible ($F = 1.9$) due to $F < 2.4$, and it was therefore excluded. We obtained the algorithm for the sea surface DMS as follows (Fig. 5(a)).

$$\begin{aligned} \ln(\text{DMS}) = & 0.06346 \cdot \text{SST} - 0.1210 \cdot \text{SSN} \\ & - 14.11 \cdot \cos(L) - 6.278 \\ (R^2 = & 0.63, p < 0.0001, \text{RMSE} = 0.65, \\ n = & 504; F = 12 \text{ for SST}, F = 35 \text{ for SSN}, \\ F = & 630 \text{ for } \cos(L)), \end{aligned} \quad (5)$$

where ' R^2 ', ' p ', ' RMSE ' and ' n ' are the coefficient of determination, the probability at a 95% confidence level, the root mean standard error of regression and the number of samples, respectively.

This algorithm can explain 63% of the variance of sea surface DMS with RMSE of 1.9 nM over the North Pacific in the last three decades, without using Chl. The sensitivity of our algorithm to each parameter between 25°N and 55°N was 0.1 nM/°C, 0.2 nM/ μM -SSN and 0.3 nM/degree-L, which was derived from the coefficient of each parameter in Eq. (5). Our algorithm

of DMS largely depends on $\cos(L)$ as a function of latitude. Kettle *et al.* (1999) showed that the sea surface DMS had a good correlation with latitudinal position from 25°N to 70°N although there are no similar correlations on a global scale. Some studies have also reported no correlation between sea surface DMS and Chl (e.g., Watanabe *et al.* 1995b). Thus the selection of parameters in our algorithm could be adequate to reconstruct the sea surface DMS in the North Pacific.

We have compared our DMS algorithm with a previous study's algorithm, which yielded results being the most similar to the observational DMS (Simó and Dachs 2002). The algorithm of Simó and Dachs (2002) was based on the ratio of Chl and the surface mixed layer depth with a difference of $0.125\sigma_\theta$ from the surface density (MLD, m). Thus, we here used the same data set of Chl as used to construct our DMS algorithm (see Subsection 3.2.2). In these observational data positions, we calculated the monthly MLD based on the climatological monthly data of temperature and salinity from World Ocean Atlas 2001 (WOA 2001) (Stephens *et al.* 2002; Boyer *et al.* 2002). Applying the above Chl and MLD into their algorithm, we compared the results of the sea surface DMS between theirs and our algorithm. Their algorithm led to significant scatter ($R^2 = 0.19$, $\text{RMSE} = 0.96$, $n = 504$) (Fig. 5(b)), suggesting that our algorithm is more advantageous way than the previous other ones due to $R^2 = 0.63$ for our algorithm, in order to reconstruct the spatiotemporal distribution of the sea surface DMS over the North Pacific.

Furthermore, evaluating the usefulness of our algorithm of sea surface DMS in the North Pacific, we tried to apply our algorithm to the independent observational data of sea surface DMS, the eastern Pacific (EP) line data along 140°W from 25°N to 55°N (April–May in 1993, $n = 163$) (Bates and Quinn 1997) which were not used to obtain Eq. (5), because this region was

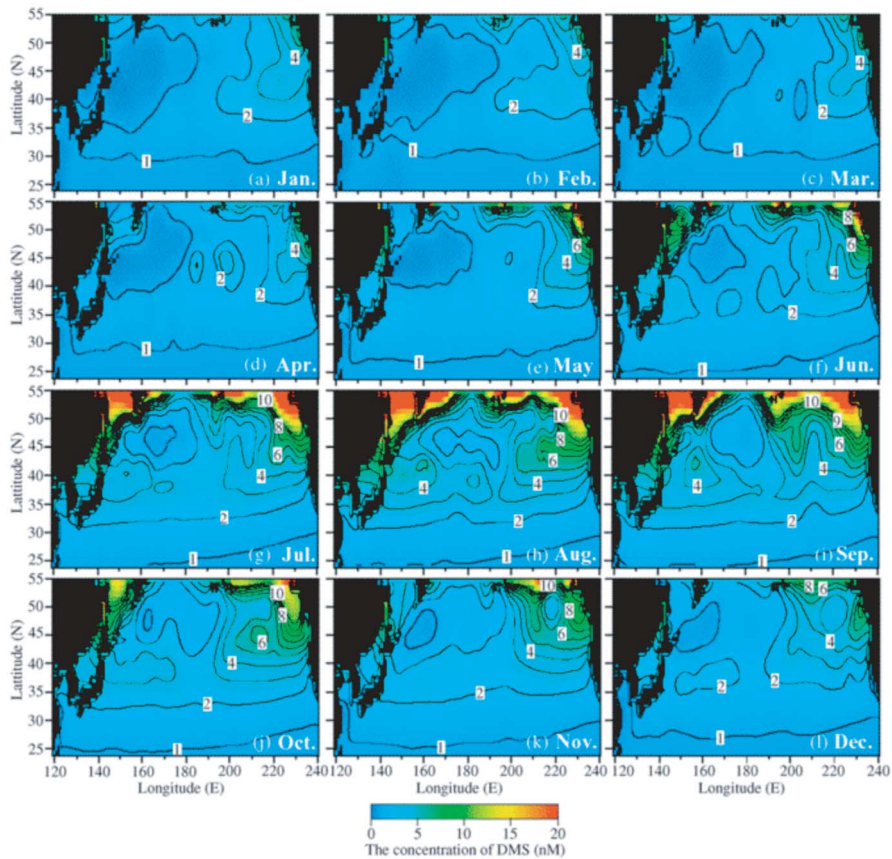


Fig. 6. Climatological distributions of monthly sea surface DMS_p (nM) in the North Pacific between 25°N and 55°N . These results were reconstructed by using Eq. (5) with climatological monthly SST and SSN of World Ocean Atlas 2001 (Stephens *et al.* 2002; Conkright *et al.* 2002).

covered by the construction of our algorithm (Fig. 4 and Table 2). We here used an empirical equation for SSN derived from SST and Chl (Goes *et al.* 2000) in order to apply SSN to Eq. (5) because the EP line had no SSN data despite being of the dataset of SST and Chl. In both the observed and predicted DMS, we found that an averaged concentration of sea surface DMS increased northward in EP line (Fig. 5(a)), which were consistent with the general previous work (Kettle *et al.* 1999). The predicted DMS agreed with these independent observational data of sea surface DMS within the uncertainty of our

approach as discussed in the above section, suggesting that our algorithm for sea surface DMS is useful over the North Pacific, at least in the region from 25°N to 55°N .

(2) Reconstruction of climatological monthly sea surface DMS in the North Pacific using WOA 2001

To understand the climatological distributions of the sea surface DMS and its flux is an essential step for clarifying the long-term changes of DMS in the North Pacific. Thus we estimated the monthly mean concentration of sea surface DMS in the North Pacific by using the climatological monthly mean dataset of

SST and SSN from WOA 2001 (Stephens *et al.* 2002; Conkright *et al.* 2002) with our DMS algorithm (Fig. 6). In the North Pacific, the concentration of sea surface DMS generally increased eastward and northward. DMS in the northeastern region is 2–5 times greater than that in the southwestern region, which agrees with the previous observational works (e.g., Kettle *et al.* 1999). In addition, we found that the concentration of sea surface DMS in the later half of the year (July–December) was 2–4 times greater than that in the first half of the year (January–June). In this period, DMS in the northeastern region remarkably increases by more than 10 nM while DMS almost did not change in the southwestern region, which agreed with previous observational results (Kettle *et al.* 1999; Wong *et al.* 2005). We estimated that the annual mean concentration of sea surface DMS was 2.2 nM between 25°N and 55°N in the North Pacific, which was equal to that of the previous observational work (Kettle *et al.* 1999). In general, larger size phytoplanktons such as *diatoms* are dominant to other species in the North Pacific. The concentration of silicate in the North Pacific surface mixed layer decreases eastward (Conkright *et al.* 2002), and consequently the abundance of phytoplanktons with calcification such as *coccolithophorids* increases eastward (e.g., Honda 2003). Compared with the western North Pacific, in the eastern North Pacific region where low diatom production and high calcification occurs (e.g., Wong *et al.* 2002), the increase of phytoplanktons with calcification such as *coccolithophorids*, seems to bring a higher concentration of sea surface DMS. In the first half of the year, diatoms bloom and their biomass decreases with the depletion of silica and/or iron. In the second half of the year, smaller-size phytoplanktons such as *coccolithophorids* become dominant instead of *diatoms* (e.g., Honda *et al.* 2002). The difference of phytoplankton species as

a producer group of DMS (e.g., Malin and Kirst 1997) between the eastern and western regions may mainly cause the spatiotemporal distribution of DMS in the North Pacific.

According to Fig. 6, multiplying the monthly DMS_p with the climatological monthly wind data at 10 m height calculated from the NCEP/NCAR reanalysis data (NCEP/NCAR 2006), the gas transfer velocity according to Wanninkhof and McGillis (1999), and the Schmidt number calculated according to Saltzman *et al.* (1993), and integrating the above estimation between 25°N and 55°N in the North Pacific, we have calculated the annual total flux of DMS from sea to air (F_{DMS}) over this region. In this region, we estimated the climatological seasonal F_{DMS} to be 0.08 Tg-S yr⁻¹ (T=10¹²) from January to March, 0.07 Tg-S yr⁻¹ from April to June, 0.15 Tg-S yr⁻¹ from July to September, and 0.17 Tg-S yr⁻¹ from October to December, indicating that F_{DMS} in the later half of the year (July–December) is about 70% of the total annual flux of DMS over this region (0.47 Tg-S yr⁻¹). In this region that corresponds to 8% of global ocean's area, the climatological annual total flux of DMS from sea to air was found to be 1–3% of the global flux of DMS predicted in previous works (e.g., Bates *et al.* 1992; Watts 2000), which is smaller than the global mean flux of DMS per area. The main reason may be due to the exiguity of small-size species as a high-producer group of DMS (e.g., Malin and Kirst 1997) compared to the North Atlantic Ocean despite this region having one of the largest primary productivity derived from the diatom species (e.g., Honda *et al.* 2002).

(3) Decadal changes of sea surface DMS

Understanding the possibility of a decadal change of DMS in the ocean is an important step towards clarifying the impact of DMS flux from sea to air on global warming. However, it may be difficult for the present DMS algorithms to estimate the

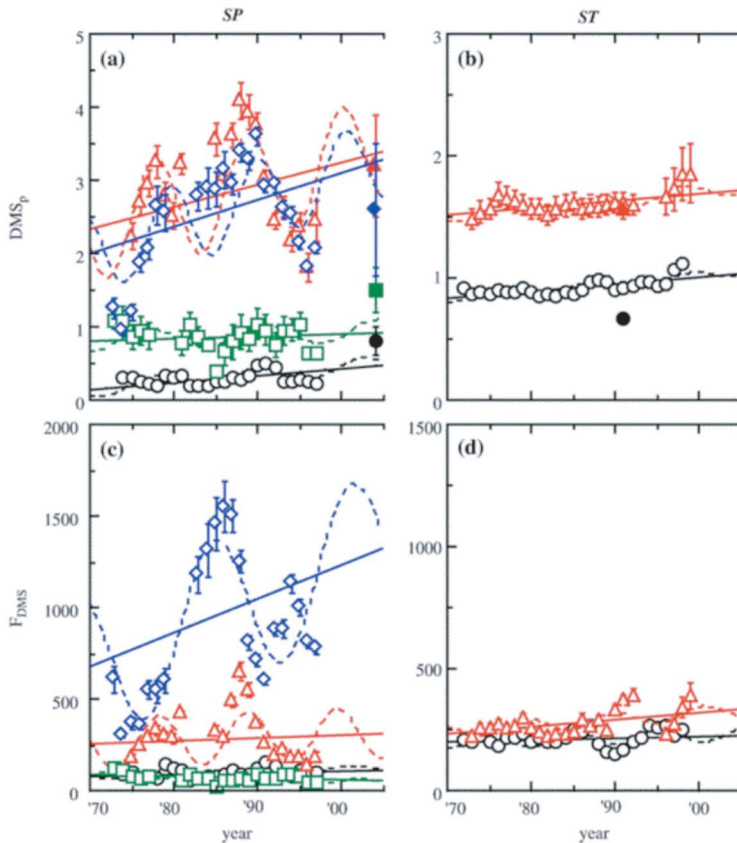


Fig. 7. Time series of DMS_p (nM) and FDMS ($\mu\text{mol m}^{-2} \text{year}^{-1}$) in SP and ST regions of the western North Pacific. DMS_p was estimated by substituting SST and SSN in the time series datasets for Eq. (5). We also estimated FDMS by multiplying DMS_p with the seasonal wind data at 10 m height from the NCEP/NCAR reanalysis data (NCEP/NCAR Reanalysis Project 2006), the gas transfer velocity according to Wanninkhof and McGillis (1999), the Schmidt number calculated according to Saltzman *et al.* (1993). We showed an averaged value as 3-year running mean composites with the standard error (SE) (J–M: black open circles; A–J: green open squares; J–S: red open triangles; O–D: blue open diamonds). Each solid symbol with SE is the averaged value of sea surface DMS observed in the same region in 2004 in SP region and in 1991 in ST region, which was not used to obtain our DMS algorithm. We also showed the linear regression line (solid line) and the non-linear fitting curve (dotted curve) which was estimated by the Fourier sine expansion with a 95% confidence level. (a) DMS_p in SP region. (b) DMS_p in ST region. (c) FDMS in SP region. (d) FDMS in ST region. The linear increasing trends of DMS_p and FDMS were significantly found as follows: DMS_p (J–M) in SP = $0.01 \text{ nM year}^{-1}$ ($p < 0.01$); DMS_p (J–S) in SP = $0.03 \text{ nM year}^{-1}$ ($p < 0.05$); DMS_p (O–D) in SP = $0.04 \text{ nM year}^{-1}$ ($p < 0.01$); DMS_p (J–M) in ST = $0.01 \text{ nM year}^{-1}$ ($p < 0.01$); DMS_p (J–S) in ST = $0.01 \text{ nM year}^{-1}$ ($p < 0.01$). FDMS (J–M) in SP = $1.4 \mu\text{mol m}^{-2} \text{year}^{-1}$ ($p < 0.05$); FDMS (A–J) in SP = $-1.1 \mu\text{mol m}^{-2} \text{year}^{-1}$ ($p < 0.05$); FDMS (O–D) in SP = $18.8 \mu\text{mol m}^{-2} \text{year}^{-1}$ ($p < 0.01$); FDMS (J–M) in ST = $0.9 \mu\text{mol m}^{-2} \text{year}^{-1}$ ($p < 0.05$); FDMS (J–S) in ST = $2.8 \mu\text{mol m}^{-2} \text{year}^{-1}$ ($p < 0.01$).

decadal change of DMS. Even in our algorithm of DMS, there was a large error of 1.9 nM. If we try to apply our algorithm to an arbitrary fixed ocean observational point, the third term of right-hand side ($\cos(L)$) in Eq. (5) of our algorithm can be considered as a constant in time although both SST and SSN have temporal changes. The relative error of $\cos(L)$ becomes zero. Consequently, if we focus on the relative temporal change of sea surface DMS in arbitrary fixed observational point, RMSE can decrease by 0.7 nM in our algorithm, which is about one third compared with the original RMSE in our algorithm. Thus, it may allow us to estimate the decadal change of the sea surface DMS in an arbitrary fixed observational point by using our algorithm of DMS.

We have applied our algorithm to the time series data of hydrographic parameters including SST and SSN in the subpolar (SP) and subtropical (ST) regions in the western North Pacific from 1971 to 2000 that was conducted by JMA (2001) (Fig. 4 and Table 2), which is also available from the Japan Oceanographic Data Center (<http://www.jodc.go.jp/service.htm>). In the SP region, the R/V Kofu-Maru has conducted the hydrographic observations 4–5 times a year at one degree interval along 42°N in the Oyashio region. In general, in the western North Pacific subpolar region, we can find the largest phytoplankton bloom from April to June and the strongest stratification of the surface mixed layer from July to September (e.g., Tsurushima *et al.* 2002). Thus we divided the time series data into four seasonal periods: January–March (J–M), April–June (A–J), July–September (J–S), October–December (O–D). On the other hand, in ST region, the R/V Ryofu-Maru has observed the hydrographic data at one degree interval from 25°N to 34°N along 137°E in the winter (January–February (J–M)) and the summer (August–September (J–S)). We addressed an aver-

aged seasonal value of each parameter (SST and SSN) in the two regions, which was expressed as three-year running mean composites with standard errors (SE, $\pm 1\sigma$) for neglecting large anomaly of DMS arising from anomalies of the observed SST and SSN.

We have demonstrated the temporal change of sea surface DMS (DMS_p) reconstructed in each season in the western North Pacific by using Eq. (5) (Figs. 7(a) and (b)). To confirm the temporal usefulness of our algorithm, we also plot the independent observational data of sea surface DMS (DMS_o) (2004 in SP region; 1991 in ST region) in each season (Figs. 7(a) and (b), Table 2), which were not used to obtain Eq. (5). In SP region, an averaged difference between DMS_p and DMS_o was 0.3 ± 0.01 nM, and DMS_p in all seasons was consistent with DMS_o within RMSE of 0.7 nM. On the other hand, in ST region, we found that DMS_p agreed with DMS_o within the difference of 0.2 ± 0.1 nM, which was also consistent with DMS_o within RMSE of 0.7 nM although DMS_p in wintertime was slightly higher than DMS_o due probably to an insufficiency of wintertime data for constructing our algorithm and due to low SSN values close to the detection limit. Considering the above results, it is possible that our algorithm could be useful for reconstructing the decadal change of sea surface DMS in the western North Pacific.

We tried to clarify the decadal changes of DMS in the western North Pacific. In both SP and ST regions, we found that the climatological averaged value of DMS_p from July to December was significantly higher (average: SP region = 2.8 ± 0.1 nM; ST region = 1.5 ± 0.02 nM) than that from January to June (average: SP region = 0.7 ± 0.1 nM; ST region = 0.9 ± 0.01 nM). In general, *diatoms* are dominant to other species in the North Pacific. In the first half of the year, they bloom and their biomass decreases with the depletion of silica and/

or iron. In the second half of the year, smaller size phytoplanktons such as *coccolithophorids* become dominant instead of diatoms (e.g., Honda *et al.* 2002). In addition, from the first to the second half of the year, Imai *et al.* (2002) found a remarkable decrease of larger-size phytoplankton (>10 μm fraction) from 34% to 8% in the western North Pacific. The differences of sea surface DMS between the first and second half of the year, may be influenced by the seasonal change of different phytoplankton species.

Moreover, we here focused on the long-term trend of sea surface DMS. By using a simple linear regression, DMS_p has significantly shown an averaged linear increase of $0.03 \pm 0.01 \text{ nM yr}^{-1}$ in SP region ($p < 0.01$), and $0.01 \pm 0.001 \text{ nM yr}^{-1}$ in ST region ($p < 0.01$), indicating that the sea surface DMS has increased by 0.9 nM in SP region, and by 0.3 nM in ST region during the past three decades. Even if considering RSME of 0.7 nM in our algorithm, DMS in SP region significantly had shown a linear increasing trend at least in the last three decades while DMS in ST region may increase although not significantly. In both regions, some studies reported that water temperature has increased by $0.2\text{--}1.5^\circ\text{C yr}^{-1}$ and the concentration of nitrate has decreased by $0.3\text{--}1.5 \mu\text{M yr}^{-1}$ in the past three decades (Watanabe *et al.* 2003, 2005; Chiba *et al.* 2004). Because the sensitivity of DMS in our algorithm between 25°N and 55°N has $0.1 \text{ nM}/^\circ\text{C}$ and $0.2 \text{ nM}/\mu\text{M-SSN}$ respectively, the changes in these parameters can explain 75% of an averaged increase of DMS in the two regions in the past three decades in the case of maximum decadal changes of water temperature and nitrate. This suggests that our algorithm is almost useful for constructing the spatiotemporal distribution of sea surface DMS, at least in the western North Pacific.

In order to clarify the extent of decadal periodicity of DMS with the long-term linear trend, according to previous studies

(Ono *et al.* 2001; Watanabe *et al.* 2003, 2005), we assumed that the long-term change of sea surface DMS can be expressed by the Fourier sine expansion as follows:

$$\text{DMS} = h \cdot y + i + j \cdot \sin\{2\pi(y - k)/l\}, \quad (6)$$

where 'y' is the calendar year, 'h'-'l' are constants. Applying this equation to the time series of DMS_p in Fig. 7, we found an averaged periodicity of 11.9 ± 0.5 years in the two regions ($R = 0.70 \pm 0.05$, $p < 0.05$), superimposed on the above linear increasing trend. Although the periodicity of DMS has been slightly shorter than those of O_2 , PO_4 and Chl over the North Pacific (oscillation of about 18 years) (Ono *et al.* 2001; Watanabe *et al.* 2003, 2005), the increasing trend of DMS seemed to be opposite to the temporal decreasing trends in diatom and zooplankton biomass (Chiba *et al.* 2004). The decreases of diatom and zooplankton biomass may affect the increase of sea surface DMS due to the increase of smaller-size phytoplankton as a high producer group of DMS and the decline of grazing effect of zooplankton, although it is difficult to explain clearly the cause of decadal periodicity of DMS due to the complicated changes of the hydrographic biogeophysical parameters.

Recent reports showed that Chl has declined in the past three decades in both the subpolar and subtropical regions in the western North Pacific due to a weakening of the surface-deep water mixing (Watanabe *et al.* 2001, 2005; Gregg and Conkright 2002; Chiba *et al.* 2004), indicating the decrease of larger-size phytoplankton as *diatoms* (Chiba *et al.* 2004). The weakening of the surface-deep water mixing was caused by both an increasing temperature and a decreasing salinity in the two regions (Ono *et al.* 2001; Andreev and Watanabe 2002; Watanabe *et al.* 2003, 2005). Consequently, MLD has shoaled although the long-term trend of

MLD has been not significant due to large variation, and the nutrients in the surface mixed layer have decreased (Watanabe *et al.* 2005). In addition, some studies have already reported that the blooms of phytoplankton producing DMS tend to be restricted in shallower mixed layer (e.g., Malin and Kirst 1997). Karl *et al.* (2001) and Ishida *et al.* (2009) also showed the possibility of a domain shift of phytoplankton from larger-size to smaller-size in the North Pacific in the past several decades. In the high latitude of North Pacific, smaller-size phytoplanktons such as *coccolithophorids* may tend to be dominant with a decline of the grazing effect of zooplankton instead of diatoms (e.g., Chiba *et al.* 2004). Thus, the linear increasing trend of sea surface DMS with the decadal periodicity may be caused by the above domain shift of phytoplankton derived from the weakening of the surface-deep water mixing in the North Pacific.

Furthermore, we estimated the decadal change in flux of DMS from sea to air (F_{DMS}) in SP and ST regions, by multiplying DMS_p with the seasonal wind data at a 10 m height from the NCEP/NCAR reanalysis data (NCEP/NCAR 2006), the gas transfer velocity according to Wanninkhof and McGillis (1999), the Schmidt number calculated according to Saltzman *et al.* (1993) and Eq. (5) (Figs. 7(c) and (d)). We found that the annual averaged F_{DMS} was $248 \pm 10 \mu\text{mol m}^{-2} \text{yr}^{-1}$ in ST region, and $336 \pm 53 \mu\text{mol m}^{-2} \text{yr}^{-1}$ in SP region. In the later half of the year, we found a higher averaged F_{DMS} over $250 \mu\text{mol m}^{-2} \text{yr}^{-1}$ in both regions (J–S in ST region = $280 \pm 10 \mu\text{mol m}^{-2} \text{yr}^{-1}$; J–S in SP region = $303 \pm 30 \mu\text{mol m}^{-2} \text{yr}^{-1}$; O–D in SP region = $872 \pm 81 \mu\text{mol m}^{-2} \text{yr}^{-1}$), which arose from the high content of DMS, the low Schmidt number and/or the strong wind speed. In the second half of the year in the past thirty years, the linear trend of F_{DMS} has increased by $2.8 \mu\text{mole m}^{-2} \text{yr}^{-1}$ in ST region ($p < 0.01$),

and by $18.8 \mu\text{mole m}^{-2} \text{yr}^{-1}$ in SP region ($p < 0.01$), which was equal to the seasonal rate of increase of 1–2% of the climatological seasonal averaged F_{DMS} in the two regions. Converting the above seasonal linear increasing trends of F_{DMS} into annual averages, we estimated a linear increase of $1.9\text{--}4.8 \mu\text{mole m}^{-2} \text{yr}^{-1}$, which was equal to the annual rate of increase of about 1% of the climatological annual averaged F_{DMS} in the two regions in the last three decades in the western North Pacific.

Concluding remarks

We established an empirical equation of the sea surface DMS (nM) using the sea surface temperature (SST, K), the sea surface nitrate (SSN, μM) and the latitude (L, $^{\circ}\text{N}$) to reconstruct the sea surface flux of DMS over the North Pacific between 25°N and 55°N : $\ln\text{DMS} = 0.06346 \cdot \text{SST} - 0.1210 \cdot \text{SSN} - 14.11 \cdot \cos(L) - 6.278$ ($R^2 = 0.63$, $p < 0.0001$).

Applying our algorithm to climatological hydrographic datasets in the North Pacific, we reconstructed the climatological monthly distribution of DMS. We found that the concentration of sea surface DMS generally increased eastward and northward, and DMS in the northeastern region became 2–5 times as large as that in the southwestern region. The concentration of DMS in the latter half of the year (July–December) was 2–4 times as large as that in the first half of the year (January–June).

Furthermore, applying our algorithm to hydrographic time series datasets in the western North Pacific from 1971 to 2000, we demonstrated that the sea surface DMS over the last three decades has shown the linear increasing trends of $0.03 \pm 0.01 \text{ nM yr}^{-1}$ in the subpolar region, and $0.01 \pm 0.001 \text{ nM yr}^{-1}$ in the subtropical region, indicating that the annual flux of DMS from sea to air has increased by $1.9\text{--}4.8 \mu\text{mol m}^{-2} \text{yr}^{-1}$ in the western North Pacific. The increase was equal to the annual rate of in-

crease of about 1% of the climatological annual averaged F_{DMS} in the western North Pacific in the last three decades.

Satellite measurements have recently reproduced a detailed spatiotemporal distribution of SST, Chl and the wind speed. On the other hand, Goes *et al.* (2000) has already reported an algorithm of SSN derived from SST and Chl with high precision. Using satellite data with their SSN algorithm, our algorithm will enable us to estimate the detailed spatiotemporal distributions of sea surface DMS and its flux over the North Pacific, and to detect the detailed seasonal change and decadal trend of DMS in the future.

However, it may be difficult to apply our present algorithm to the future prediction of DMS due to insufficient observational time-series of DMS with other hydrographic parameters. It would be necessary to improve the algorithm of DMS based on the many observational data. To improve the algorithm, an essential step would be to collect DMS data equipped with multiple hydrographic parameters such as chlorophyll-a, water temperature and nutrients from the data centers having many hydrographic observational data (e.g., NOAA 2006). Unfortunately, there were actually few datasets of multiple hydrographic parameters with DMS data in the data centers. In the future, it will be necessary to continue collecting accurate and long time series data of DMS with other hydrographic parameters over the North Pacific in order to predict the effect of DMS on global warming.

Influence of Riverine Alkalinity on Carbonate Species in the Okhotsk Sea

With the recent increase of atmospheric CO_2 , a decrease of pH in the ocean surface water will be caused. Some ocean observations have also shown a decreasing trend of pH during recent decades in the open oceans. On the other hand, in the

marginal seas, some investigators also reported the decadal increase of dissolved inorganic carbon, suggesting a possibility that pH could decrease in these regions as well as in the open ocean. However, the change of pH has still not been reported throughout the land-river-ocean system containing the continental marginal seas. Here we focused on the Okhotsk Sea as a large marginal sea to evaluate the extent of change in pH during recent decades.

Introduction

A recent model calculation predicts that a decrease of pH in the ocean surface water will be caused as a response to an increase of atmospheric CO_2 in the future (e.g., Orr *et al.* 2005). Some ocean observations have also shown a decreasing trend of $0.4 \pm 0.4 \mu\text{mol kg}^{-1} \text{y}^{-1}$ for alkalinity (Alk) and that of $0.0019 \pm 0.0003 \text{y}^{-1}$ for pH during recent decades in the Pacific and the Indian Oceans (Sarma *et al.* 2002; Feely *et al.* 2008). However, these results were estimated based on carbonate species data that have large errors and/or assumptions of no land-ocean interactions with increasing temperature. In the North Atlantic marginal seas and the South China Sea, some investigators also reported the decadal increase of dissolved inorganic carbon (DIC) (e.g., Thomas *et al.* 2007), suggesting a possibility that pH could decrease in these regions as well as the open ocean. However, a change of pH has still not been reported throughout the land-river-ocean system containing the continental marginal seas.

On the other hand, IPCC (2007) reported that global warming has recently been led to changes in the global ocean environment. In the North Pacific, several studies have also reported the same trends as the global one, which has been caused by the weakening of formation/circulation of North Pacific Intermediate Water (NPIW) as a response to the reinforcement of ocean stratification (e.g., Watanabe *et*

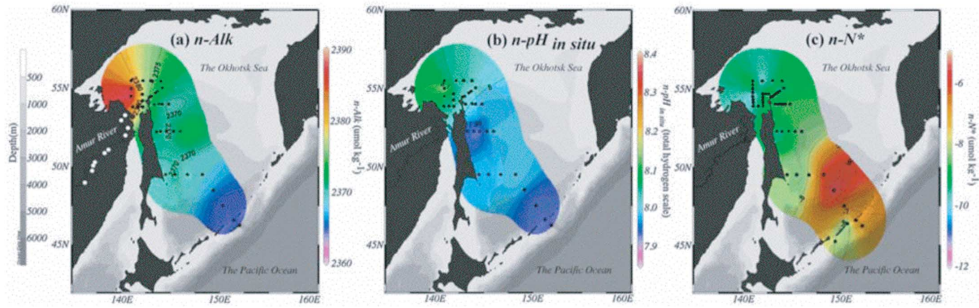


Fig. 8. Distributions of (a) $n\text{-Alk}$, (b) $n\text{-pH}$ in situ and (c) $n\text{-N}^*$ on $26.5\sigma_\theta$ in 2006. Black and white circles are the oceanic and riverine sampling locations. Using these pairs of $n\text{-Alk}$ and $n\text{-DIC}$, we calculated the $n\text{-pH}$ in situ based on Dickson and Goyet (1994). We used the Ocean Data View (Schlitzer 2007, <http://odv.awi.de>).

al. 2001). NPIW is centered on $26.8\sigma_\theta$, which is the only water mass produced in the North Pacific, influencing the climate of the North Pacific. One of the origins is in the Okhotsk Sea. Dense shelf water (DSW) is produced by brine rejection during sea ice formation in the continental shelves and joins rapidly with Okhotsk Sea Intermediate Water (OSIW). OSIW has a ventilation time of several years, and is transported into NPIW (e.g., Ohshima and Martin 2004). In addition, snowmelt water and/or monsoon derived rainwater in Siberia bring inflows of high contents of Alk and nutrients into the Okhotsk Sea through the Amur River of which the catchment area is the tenth largest in the world (Andreev and Pavlova 2010). This region may have a probability of the recent changes in carbonate species influenced by land-river-ocean interactions as well as recent anthropogenic perturbations. In 2006, we thus revisited the same observation area as examined in 1999 and 2000 in the Okhotsk Sea, and observed the same hydrographic properties to clarify the degree of change of pH with other hydrographic parameters in the Okhotsk Sea.

Data and methods

On the R/V Professor Khromov, we

obtained the samples of hydrographic chemical properties from 0 m to 3000 m depth at 34 stations for Alk and DIC, and at 51 stations for nutrients (NH_3 , NO_2 , NO_3 , PO_4 , $\text{Si}(\text{OH})_4$, DO) during August to early September in 2006, covering the formation area of intermediate water in the Okhotsk Sea (Fig. 8). Sampling and measurement methods for each observed property were carried out according to the JGOFS and DOE protocols (DOE 1994; Knap *et al.* 1996). In the Amur River, we observed Alk at 10 stations of even intervals from about 1000 km upriver to the mouth of the river in September 2005 (Fig. 8(a)) and measured them by using the one-point titration method of Ono *et al.* (1998). Certified reference materials of Alk and DIC distributed by Prof. A. G. Dickson (Scripps Inst. Oceanogr.) were used. These were the same procedures as used in the summer of 1999 (July) and 2000 (August). In the same sampling region, data of each property in 2006 were compared to those in 1999 and 2000 by using an isopycnal grid analysis. In the continental shelves of the northern part in summer, a heterogeneous remnant of water mass developed in winter sometimes exists with a minimum of water temperature (θ) above $26.8\sigma_\theta$ (e.g., Wakita *et al.* 2003). We thus neglected water mass with $\theta \leq -1.5^\circ\text{C}$ and

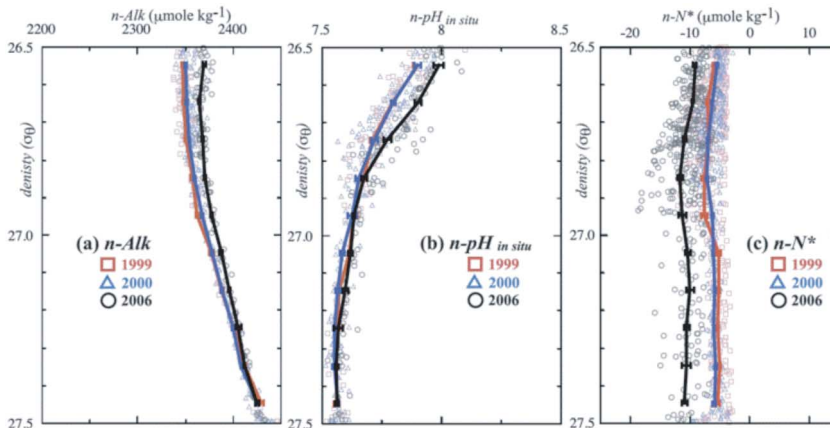


Fig. 9. Average vertical distributions of $n\text{-Alk}$, $n\text{-pH}_{in\ situ}$ and $n\text{-N}^*$ in the Okhotsk Sea among 1999 (red square), 2000 (blue triangle) and 2006 (black circle) with standard errors. The solid line is an average value of each property on each isopycnal horizon.

$\theta \cong 26.8$ as an anomaly. In addition, we assumed that water mass below $27.4\sigma_\theta$ has not changed on a decadal time scale, since recent transient tracers such as chlorofluorocarbons have still not been found below $27.4\sigma_\theta$ over the Okhotsk Sea throughout the 1990s (Yamamoto-Kawai *et al.* 2004). By estimating the difference of each property between each cruise based on the deep-water data sets below $27.4\sigma_\theta$ in 2000, both Alk and DIC had offsets of $3 \pm 1 \mu\text{mol kg}^{-1}$. The offset values of NH_3 , NO_2 , NO_3 , PO_4 , $\text{Si}(\text{OH})_4$ and DO were within $0.1 \mu\text{mol kg}^{-1}$, $0.02 \mu\text{mol kg}^{-1}$, $1 \mu\text{mol kg}^{-1}$, $0.1 \mu\text{mol kg}^{-1}$, $5 \mu\text{mol kg}^{-1}$, and $1 \mu\text{mol kg}^{-1}$, respectively. While the offsets of nutrients were sufficiently small, it was necessary to make corrections for the offsets of carbonate species in order to clarify these changes. We here made corrections for the offsets of Alk and DIC by subtracting each offset from the raw data.

Using these pairs of Alk and DIC, we calculated the $\text{pH}_{in\ situ}$ temperature ($\text{pH}_{in\ situ}$: total hydrogen scale) based on DOE (1994). Furthermore, in order to estimate the degree of change of the nitrogen cycle that can affect the contents of Alk and $\text{pH}_{in\ situ}$,

in situ, we estimated N^* ($=[\text{NO}_3] + [\text{NO}_2] + [\text{NH}_3] - r_{\text{N/P}}[\text{PO}_4] + 2.9$ (e.g., Yoshikawa *et al.* 2006)) as an index of nitrogen fixation-denitrification by using the observed nutrient data. The positive and negative values of N^* imply the possibilities of nitrogen-fixation and denitrification. In the case of focusing on the relative change of N^* among 1999, 2000 and 2006, a value for the stoichiometric ratio of N to P ($r_{\text{N/P}}$) is not critical. Since there is a high concentration of iron in this region (Nishioka *et al.* 2007), a possibility that $r_{\text{N/P}}$ changes during this period would be small. We therefore used $r_{\text{N/P}} = 16$. In order to avoid the change of water mass in the isopycnal grid analysis, we also addressed all the data by normalizing them to salinity of 35 using the optimal salinity-normalization scheme with a non-zero freshwater endmember (Friss *et al.* 2003), which were shown with the prefix ‘ n ’. As a non-zero freshwater endmember, we here assumed $\text{Alk} = 589 \mu\text{mol kg}^{-1}$, $\text{DIC} = 294 \mu\text{mol kg}^{-1}$, $\text{AOU} = 0 \mu\text{mol kg}^{-1}$ and $\text{N}^* = 0 \mu\text{mol kg}^{-1}$ based on the climatological riverine data (Andreev and Pavlova 2010).

Table 3. Average increasing rates of salinity-normalize properties from 1999 to 2006, R_{n-Alk} , R_{n-N^*} , $R_{n-pH\ in\ situ}$ and R_{n-DIC^*} with R_{θ}^*

	R ('06-'99)	R ('06-'00)	Average
	$\langle R_{n-Alk}, \mu\text{mol kg}^{-1} \text{y}^{-1}, (\mu\text{mol kg}^{-1}) \rangle$		
26.5–26.8 σ_{θ}	2.7 (18.7)	2.5 (15.1)	2.6 \pm 0.1
26.8–27.3 σ_{θ}	1.5 (10.2)	1.4 (8.2)	1.4 \pm 0.1
27.3–27.4 σ_{θ}	-0.3 (-2.1)	0.2 (0.9)	-0.1 \pm 0.2
	$\langle R_{n-N^*}, \mu\text{mol kg}^{-1} \text{y}^{-1}, (\mu\text{mol kg}^{-1}) \rangle$		
26.5–26.8 σ_{θ}	-0.5 (-3.4)	-0.6 (-3.3)	-0.5 \pm 0.1
26.8–27.3 σ_{θ}	-0.6 (-4.4)	-0.7 (-4.5)	-0.7 \pm 0.0
27.3–27.4 σ_{θ}	-0.8 (-5.1)	-0.8 (-5.5)	-0.8 \pm 0.0
	$\langle R_{n-DIC^*} (= R_{n-DIC} - r_{-C/O_2} R_{n-AOU}), \mu\text{mol kg}^{-1} \text{y}^{-1}, (\mu\text{mol kg}^{-1}) \rangle$		
26.5–26.8 σ_{θ}	1.3 (9.3)	1.1 (6.6)	1.2 \pm 0.1
26.8–27.3 σ_{θ}	0.3 (2.0)	0.7 (4.5)	0.5 \pm 0.2
27.3–27.4 σ_{θ}	-0.2 (-1.6)	0.1 (0.7)	-0.1 \pm 0.2
	$\langle R_{n-pH\ in\ situ}, \text{pH unit y}^{-1}, (\text{pH unit}) \rangle$		
26.5–26.8 σ_{θ}	0.013 (0.089)	0.014 (0.086)	0.013 \pm 0.001
26.8–27.3 σ_{θ}	0.002 (0.012)	0.004 (0.025)	0.003 \pm 0.001
27.3–27.4 σ_{θ}	0.001 (0.004)	0.001 (0.006)	0.001 \pm 0.000
	$\langle R_{\theta}, ^\circ\text{C y}^{-1}, (^\circ\text{C}) \rangle$		
26.5–26.8 σ_{θ}	0.02 (0.16)	0.01 (0.07)	0.02 \pm 0.01
26.8–27.3 σ_{θ}	0.06 (0.39)	0.02 (0.09)	0.04 \pm 0.02
27.3–27.4 σ_{θ}	0.00 (0.00)	0.00 (-0.02)	0.00 \pm 0.00

*The value in parenthesis is the increased amount of each property during each sampling time interval. The errors showed the standard errors. The average depths of 26.5 σ_{θ} , 26.8 σ_{θ} and 27.3 σ_{θ} throughout the entire period, are 62 \pm 15 m, 234 \pm 21 m and 750 \pm 11 m, respectively.

Results

On the isopycnal horizon of 26.5 σ_{θ} as the remnant of the winter mixed layer, n -Alk decreased from the inner shelf to the offshore (Fig. 8(a)), indicating that the Amur River and the continental shelf significantly affect the spatial distributions of carbonate species in the Okhotsk Sea (e.g., Wakita *et al.* 2003). Similarly, n -DIC and n -pH_{*in situ*} decreased to the offshore while n -N* increased (Figs. 8(b) and (c), n -DIC not shown). Comparing the isopycnal averaged values of all the salinity-normalized hydrographic properties during this period, we found significant changes of n -Alk, n -pH_{*in situ*} and n -N* in the subsurface water (Fig. 9 and Table 3, see Fig. 8 for the calculation of n -pH_{*in situ*}). Although the variations of these properties gradually changed from the inner shelf to the offshore, since the observation area and the sampling points were the same throughout 1999, 2000 and 2006, we estimated the average rates of change of n -Alk (R_{n-Alk})

and n -pH_{*in situ*} ($R_{n-pH\ in\ situ}$), which increased by 2.6 $\mu\text{mol kg}^{-1} \text{y}^{-1}$ and 0.013 pH unit y^{-1} , respectively. $R_{n-pH\ in\ situ}$ was significantly larger than the effect of offset corrections (0.005 \pm 0.003 pH unit). On the other hand, the rate of n -N* (R_{n-N^*}) was from -0.8 to -0.5 $\mu\text{mol kg}^{-1} \text{y}^{-1}$. Furthermore, considering a corrected value of n -DIC from the effect of remineralization of organic carbon (n -DIC* = n -DIC - $r_{-C/O_2} n$ -AOU, where AOU and r_{-C/O_2} are the apparent oxygen utilization and the stoichiometric ratio of DIC to oxygen (Anderson and Sarmiento 1994)), we obtained that the rate of n -DIC* (R_{n-DIC^*}) increased by 1.2 $\mu\text{mol kg}^{-1} \text{y}^{-1}$ above 27.3 σ_{θ} , which was almost half of R_{n-Alk} (Table 3). Using these pairs of R_{n-Alk} and R_{n-N^*} on 26.5 σ_{θ} with the atmospheric CO₂ increment during this period, we estimated that R_{n-DIC^*} caused by the increase of atmospheric CO₂ was 0.5 \pm 0.1 $\mu\text{mol kg}^{-1} \text{y}^{-1}$, indicating that the residue of R_{n-DIC^*} was about half of R_{n-Alk} excluding the influence

of R_{n-N^*} . We also found that Alk in the Amur River was almost constant throughout the Amur River, $1867 \pm 26 \mu\text{mol kg}^{-1}$.

The above trends contained the natural variations and the long-term trends, and it is difficult to distinguish between them due to only three observational data sets in our study. However, it is important to clarify the extent of influences of these changes in this region on ocean acidification in the North Pacific. In the following sections, we will discuss the changes in these properties without making a distinction between the natural and the long-term changes.

Discussion

(1) Factors changing Alk and $\text{pH}_{in situ}$ in the Okhotsk Sea

In order to explain the significant increases of Alk and $\text{pH}_{in situ}$ in the subsurface water, we can consider the following causes: (i) the decrease of θ ; (ii) the changes in the mixing between the Okhotsk Sea and the Pacific and/or the vertical mixing; (iii) the strengthening of CaCO_3 dissolution; (iv) the reinforcement of denitrification; and (v) the increase of Ca^{2+} derived from an exterior system of the Okhotsk Sea.

Our study showed an increasing rate of θ of $0.02\text{--}0.04^\circ\text{C y}^{-1}$ above $27.3\sigma_\theta$ (Table 3), causing the decrease of $\text{pH}_{in situ}$ of $0.001 \text{ pH unit y}^{-1}$, rather than an increase of $\text{pH}_{in situ}$. The value of $n\text{-Alk}$ in the North Pacific is lower than that in the Okhotsk Sea (Fig. 8(a)). The recent reinforcement of ocean stratification in the Okhotsk Sea has already been reported (e.g., Osafune and Yasuda 2006). In our study, the increasing rates of the saturation states of aragonite and calcite were only 0.03 y^{-1} and 0.05 y^{-1} , respectively. $R_{n\text{-Alk}}$ with $R_{n\text{-DIC}^*}$ being half of $R_{n\text{-Alk}}$ were almost found above these saturation state depths. Furthermore, the value of $R_{n\text{-N}^*}$ can only cause about one-fifth of the observed increase of $n\text{-Alk}$, although we found $R_{n\text{-N}^*}$ from -0.8 to -0.5

$\mu\text{mol kg}^{-1} \text{ y}^{-1}$ (Table 3). Therefore, since the cases of (i)–(iv) can be ignored, the case of (v) could possibly result in most of the increases of Alk and $\text{pH}_{in situ}$ in this study.

(2) Mass balance of Alk between the Amur River and the Okhotsk Sea

As an effect derived from an exterior system of the Okhotsk Sea, one of the most probable possibilities is the increase of efflux of Ca^{2+} arising from the change of the outflow characteristics of the Amur River: the increases of riverine discharge and/or the increase of Ca^{2+} content as Alk because $R_{n\text{-Alk}}$ with $R_{n\text{-DIC}^*}$ being half of $R_{n\text{-Alk}}$ were almost found above the saturation state depths of CaCO_3 in the subsurface. We here tried to estimate the extent of these effects in the Amur River. In order to elucidate the actual net increasing rate of the water column inventory of Alk in the Okhotsk Sea ($\Delta I_{net\text{-Alk}(sea)}$, mol y^{-1}), using the observed data without salinity normalization, we need to consider R_{N^*} in addition to R_{Alk} as follows:

$$\Delta I_{net\text{-Alk}(sea)} = A \cdot 10^{-3} \int_{0 \text{ m}}^{\text{depth(m) at } 27.4\sigma_\theta} \rho_{sea(z)} \cdot (R_{Alk(z)} + R_{N^*(z)}) dz \quad (7)$$

where A , ρ_{sea} and z are the sea surface area (m^2), the sea water density (kg m^{-3}) and the water depth (m), respectively. R refers to the average rate of increase of one in the parameters of Alk and N^* observed during 1999 to 2006 ($\mu\text{mol kg}^{-1} \text{ y}^{-1}$). We estimated $\Delta I_{net\text{-Alk}(sea)}$ from 0 m to $27.4\sigma_\theta$ assuming that R between 0 m and $26.5\sigma_\theta$ equaled to that on $26.5\text{--}26.8\sigma_\theta$ (Table 3). As the value of A , we addressed the whole area of our observation to be the minimum (A_{\min} , $1.6 \times 10^{11} \text{ m}^2$) and the area of climatological annual mean ice cover to be the maximum (A_{\max} , $4.2 \times 10^{11} \text{ m}^2$) (Ohshima *et al.* 2006). As a result, we ob-

tained $\Delta I_{net-Alk(sea)}$ to be from 1.4×10^{11} to $3.6 \times 10^{11} \text{ mol y}^{-1}$.

Considering the change of Alk in the Amur River, it is necessary to estimate the mass balance of Alk in the following three cases to determine the cause $\Delta I_{net-Alk(sea)}$ from 1999 to 2006 in the Okhotsk Sea: (v-a) the content of Alk only changed; (v-b) the riverine discharge only changed; and (v-c) both the content of Alk and the riverine discharge changed. Actually, the discharge of the Amur River significantly increased over the past five years, and its average increasing rate was $2.2 \times 10^{10} \text{ m}^3 \text{ y}^{-1}$ (The Amur River data provided by ROSHYDROMET, Russia). Therefore, we tried to examine the cases of (v-b) and (v-c).

In the case of (v-b), we can $\Delta I_{net-Alk(river)}$ in terms of the change in discharge of the Amur River ($\Delta D, \text{ m}^3 \text{ y}^{-1}$) as follows:

$$\Delta I_{net-Alk(river)} = \rho_{river} \cdot C_{Alk(0)} \cdot \Delta D \cdot 10^{-3} \quad (8)$$

where ρ_{river} and $C_{Alk(0)}$ are the riverine water density (kg m^{-3}) and the climatological riverine content of Alk ($\mu\text{mol kg}^{-1}$). We used $589 \mu\text{mol kg}^{-1}$ for $C_{Alk(0)}$ based on the average data observed before 1999 (Andreev and Pavlova 2010). We $\Delta I_{net-Alk(river)}$ to be $1.3 \times 10^{10} \text{ mol y}^{-1}$ which is only 9% of the minimum value of $\Delta I_{net-Alk(sea)}$, indicating that the change in the riverine discharge only makes it not possible to explain the total increase of Alk in the Okhotsk Sea.

In the case of (v-c), we can calculate the changing riverine concentration of Alk (ΔC_{Alk}) with ΔD as follows:

$$\Delta I_{net-Alk(river)} = \rho_{river} \cdot [(C_{Alk(0)} + \Delta C_{Alk}) \cdot (D_{(0)} + \Delta D) - C_{Alk(0)} \cdot D_{(0)}] \cdot 10^{-3} \quad (9)$$

where $D_{(0)}$ is the climatological riverine discharge ($\text{m}^3 \text{ y}^{-1}$), which is $3.5 \times 10^{11} \text{ m}^3 \text{ y}^{-1}$ based on the average data observed before 1999 (Andreev and Pavlova 2010).

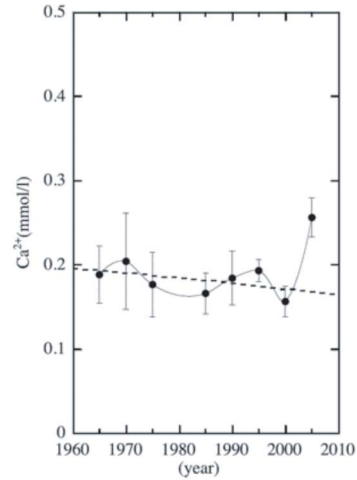


Fig. 10. Annual mean concentration of Ca^{2+} at the mouth of the Amur River in each five years from 1960 to 2005 with standard errors based on the data of the ROSHYDROMET, Russia. The dash line also shows the linear trend estimated from 1965 to 2000 although it is not significant ($p > 0.1$).

Assuming $\Delta I_{net-Alk(river)}$ to be equal to $\Delta I_{net-Alk(sea)}$, we obtained the ratio of the changing riverine content of Alk to the climatological one ($(C_{Alk(0)} + \Delta C_{Alk}) / C_{Alk(0)}$) to be from 1.6 to 2.7 times higher than the climatological riverine content of Alk. Actually, the average concentration of Ca^{2+} in the Amur River from 2000 to 2005 changed from 0.16 to 0.26 mmol l^{-1} , indicating that Ca^{2+} has increased by a factor of 1.6 (Fig. 3). In addition, we observed $1867 \pm 26 \mu\text{mol kg}^{-1}$ of Alk in the Amur River in 2005, which is 3.2 times higher than $C_{Alk(0)}$. The above results agreed with our estimation, demonstrating that the increase of Alk in the Amur River was the dominant cause for the increase of Alk in the Okhotsk Sea during 1999 and 2006.

Raymond and Cole (2003) reported a decadal increase of alkalinity in the Mississippi River derived from chemical weathering and the subsequent export from the soil to the river, which was linked to

the amount and type of land cover. In the region along the Amur River, recent industrialization and development of agriculture in Russia and China has been progressing, and deforestation and loss of wetlands also has been increasing over the past several decades (e.g., An *et al.* 2007). IPCC (2007) also reported that this area could be one of the most striking areas in the world with the air temperature increasing by more than $0.5^{\circ}\text{C}/\text{decade}$ over the last decade. Consequently, the increase of soil dissolution could be progressing. These changes along this river could cause the increase of riverine alkalinity and the subsequent increases of Alk and $\text{pH}_{in\ situ}$ in the Okhotsk Sea over the last decade.

The effect of increasing Alk and $\text{pH}_{in\ situ}$ in the Okhotsk Sea could spread over the North Pacific through the subsurface water since the water mass of the Okhotsk Sea is the origin of NPIW that influences the spatiotemporal distributions of physical and chemical properties in the North Pacific (e.g., Watanabe *et al.* 2001; Sarmiento *et al.* 2004). By considering the residence time of NPIW to be 20–30 years (e.g., Watanabe *et al.* 1994) with the increase of $n\text{-Alk}$ in this study ($1.4\text{--}2.6\ \mu\text{mol kg}^{-1}\ \text{y}^{-1}$) (Table 3), the pH in NPIW may increase by $0.0004\ \text{pH unit y}^{-1}$ although a large uncertainty is included, which could mitigate one-fifth of the ocean acidification of 0.0019 ± 0.0003 (standard error) pH unit y^{-1} ($R^2 = 0.27$) derived from anthropogenic CO_2 uptake by the ocean (Feely *et al.* 2008). Our finding indicates that this marginal sea plays a critical role in absorbing the anthropogenic CO_2 despite a predicted decrease of pH in the ocean surface waters progressing in the future. Unfortunately, based on our present data, it is difficult to determine whether the changes of Alk and $\text{pH}_{in\ situ}$ were caused by only anthropogenic perturbations or not. In order to elucidate whether oceanic pH decreases over the whole ocean, further study on the carbonate system in the

marginal seas with large rivers will enable an evaluation of the extent of future change in seawater pH.

Summary

In the above three sections (Subsection 2.4), we have demonstrated the following:

(1) Using four pentadecadal hydrographic time series of biogeochemical properties over the North Pacific subpolar region, we found that the linear trends of these properties over this region due to sea surface stratification. A decadal periodicity of 18 years was also found although there were the opposite phases between the eastern and western sides. Despite decreasing trends of DO with an increase of PO_4, N^* in the subsurface water showed an increasing trend of $0.18\ \mu\text{mol kg}^{-1}\ \text{y}^{-1}$. N^* in the surface water also showed an increase of $0.12\ \mu\text{mol kg}^{-1}\ \text{y}^{-1}$ with a decrease of Si/N. Considering the decrease of N/P, and the increase of Si/N in diatoms under iron-deficient conditions, this finding is evidence that a shift of phytoplankton has already occurred due to the progress in stratification with the depletion of iron derived from deep water, despite being a relatively high primary production region.

(2) We have proposed an empirical equation of sea surface dimethylsulfide (DMS, nM) using the sea surface temperature (SST, K), sea surface nitrate (SSN, μM) and latitude (L , $^{\circ}\text{N}$) to reconstruct the sea surface flux of DMS over the North Pacific between 25°N and 55°N : $\text{lnDMS} = 0.06346 \cdot \text{SST} - 0.1210 \cdot \text{SSN} - 14.11 \cdot \cos(L) - 6.278$ ($R^2 = 0.63$, $p < 0.0001$). Applying our algorithm to climatological hydrographic data in the North Pacific, we reconstructed the climatological distributions of DMS and its flux between 25°N and 55°N . DMS generally increased eastward and northward, and DMS in the northeastern region became to 2–5 times as large as that in the

southwestern region. DMS in the second half of the year was 2–4 times as large as that in the first half of the year. Moreover, applying our algorithm to hydrographic time series datasets in the western North Pacific from 1971 to 2000, we found that DMS over the last three decades has shown linear increasing trends of 0.03 ± 0.01 nM y^{-1} in the subpolar region, and 0.01 ± 0.001 nM yr^{-1} in the subtropical region, indicating that the annual flux of DMS from sea to air has increased by $1.9\text{--}4.8$ $\mu\text{mol m}^{-2} yr^{-1}$. The linear increase was consistent with the annual rate of increase of 1% of the climatological averaged flux in the western North Pacific over the last three decades.

(3) Comparing the data set of carbonate species and other hydrographic chemical properties in 1999, 2000 and 2006 in the Okhotsk Sea, we found that salinity-

normalized alkalinity in the subsurface water has shown a rate of increase by 2.6 ± 0.1 $\mu\text{mol kg}^{-1} y^{-1}$ while the increase in salinity-normalized dissolved inorganic carbon corrected by AOU was almost half of that in alkalinity. Therefore, pH has increased by 0.013 ± 0.001 pH unit y^{-1} in the subsurface water ($26.5\text{--}27.3\sigma_\theta$) which is the origin of the North Pacific intermediate water. This increase in pH could be explained by the increase in alkalinity in the Amur River in the last decade, suggesting the possibility that this could mitigate one-fifth of recent ocean acidification in the North Pacific.

Acknowledgements

This research has been supported by the Grant-in-Aid for Scientific Research in Priority Areas “Western Pacific Air-Sea Interaction Study (W-PASS)” under Grant No. 18067010.

References

- An S *et al.* (2007) China's natural wetlands: past problems, current status and future challenges. *Ambio* **36**: 335–342.
- Anderson LA, Sarmiento JL (1994) Redfield ratios of remineralization determined by nutrient data analysis. *Global Biogeochem. Cycles* **8**: 65–80.
- Anderson TR *et al.* (2001) Global field of sea surface dimethylsulfide predicted from chlorophyll, nutrients and light. *J. Mar. Syst.* **30**: 1–20.
- Andreae MO (1990) Ocean-atmosphere interactions in the global biogeochemical sulfur cycle. *Mar. Chem.* **30**: 1–29.
- Andreev AG, Baturina VI (2006) Impacts of tides and atmospheric forcing variability on dissolved oxygen in the subarctic North Pacific. *J. Geophys. Res.* **111**: C07S10, doi:10.1029/2005JC003103.
- Andreev AG, Pavlova GY (2010) Marginal Seas: Okhotsk Sea. In *Carbon and Nutrient Fluxes in Continental Margins* (eds. Liu KK *et al.*), Springer, Berlin, Heidelberg.
- Andreev AG, Watanabe S (2002) Temporal changes in dissolved oxygen of the intermediate water in the subarctic North Pacific. *Geophys. Res. Lett.* **29**(14): doi:10.1029/2002GL015021.
- Aranami K *et al.* (2002) Chemical assessment of oceanic and terrestrial sulfur in the marine boundary layer over the northern North Pacific during summer. *J. Atmos. Chem.* **41**: 49–66, doi:10.1023/A:103896911709.
- Aumont O *et al.* (2002) Dimethylsulfoniopropionate (DMSP) and dimethylsulfide (DMS) sea surface distributions simulated from a global three-dimensional ocean carbon cycle model. *J. Geophys. Res.* **107**(C4): doi:10.1029/1999JC000111.
- Bates TS, Quinn PK (1997) Dimethylsulfide (DMS) in the equatorial Pacific Ocean (1982 to 1996): evidence of a climate feedback. *Geophys. Res. Lett.* **24**(8): 861–864, doi:10.1029/1097GL00784.
- Bates TS *et al.* (1992) Sulfur emissions to the atmosphere from natural sources. *J. Atmos. Chem.* **14**: 315–337.
- Belviso S *et al.* (2004a) Comparison of global climatological maps of sea surface demethylsulfide. *Global Biogeochem. Cycles* **18**: GB3013, doi:10.1029/2003GB002193.
- Belviso S *et al.* (2004b) Assessment of a global climatology of oceanic dimethylsulfide (DMS) concen-

- trations based on SeaWiFS imagery (1998–2001). *Can. J. Fish. Aquat. Sci.* **61**: 804–816.
- Boyer TP *et al.* (2002) World Ocean Atlas 2001, Volume 2: Salinity. In *NOAA Atlas NESDIS 50* (ed. Levitus S), U.S. Government Printing Office, Washington, D.C., 165 pp., CD-ROMs.
- Chiba S *et al.* (2004) Increased stratification and decreased lower trophic level productivity in the Oyashio region of the North Pacific: a 30-year retrospective study. *J. Oceanogr.* **60**: 149–162.
- Chu S *et al.* (2003) Global eddy permitting simulations of surface ocean nitrogen, iron, sulfur cycling. *Chemosphere* **50**: 223–235.
- Conkright ME *et al.* (2002) World Ocean Atlas 2001, Volume 4: Nutrients. In *NOAA Atlas NESDIS 52* (ed. Levitus S), U.S. Government Printing Office, Washington D.C., 392 pp., CD-ROMs.
- Deutsch C *et al.* (2001) Denitrification and N₂ fixation in the Pacific Ocean. *Global Biogeochem. Cycles* **15**: 483–506.
- Deutsch C *et al.* (2007) Spatial coupling of nitrogen inputs and losses in the ocean. *Nature* **445**: 163–167, doi:10.1038/nature05392.
- Dickson AG, Goyet C (1994) Handbook of methods for the analysis of the various parameters of the carbon dioxide system in sea water, version 2, Rep. ORNL/CDIAC-74, Carbon Dioxide Inf. Anal. Cent., Oak Ridge, Tenn.
- DOE (1994) Handbook of methods for the analysis of the various parameters of the carbon dioxide system in sea water, version 2, ORNL/CDIAC-74.
- Emerson S *et al.* (2004) Temporal trends in apparent oxygen utilization in the upper pycnocline of the North Pacific: 1980–2000. *J. Oceanogr.* **60**: 139–147.
- Feely RA *et al.* (2008) Ocean acidification of the North Pacific Ocean. *PICES Press of the North Pacific Marine Science Organization* **16**(1): 22–26.
- Friss K *et al.* (2003) The salinity normalization of marine inorganic carbon chemistry data. *Geophys. Res. Lett.* **30**: 1085, doi:10.1029/2002GL015898.
- Goes J *et al.* (2000) Basin scale estimates of sea surface nitrate and new production from remotely sensed sea surface temperature and chlorophyll. *Geophys. Res. Lett.* **27**(9): 1263–1266, doi:10.1029/1999GL002353.
- Gregg WW, Conkright ME (2002) Decadal changes in the global ocean chlorophyll. *Geophys. Res. Lett.* **29**(15): doi:10.1029/2002GL014689.
- Hansen J *et al.* (2002) Global warming continues. *Science* **295**: 275, doi:10.1126/science.295.5553.275c.
- Honda MC (2003) Biological pump in northwestern North Pacific. *J. Oceanogr.* **59**: 671–684.
- Honda MC *et al.* (2002) The biological pump in the northwestern North Pacific based on fluxes and major components of particulate matter obtained by sediment-trap experiments (1997–2000). *Deep-Sea Res. II* **49**: 5595–5625.
- Hutchins DA, Bruland KW (1998) Iron-limited diatom growth and Si:N uptake ratios in a coastal upwelling regime. *Nature* **393**: 561–564.
- Imai K *et al.* (2002) Time series of seasonal variation of primary productivity at station KNOT (44N, 155E) in the sub-arctic western North Pacific. *Deep-Sea Res. II* **49**: 5395–5408.
- IOS (2006) IOS (Institute of Ocean Science) Line P Oceanographic Data, http://www-sci.pac.dfo-mpo.gc.ca/osap/data/linep/linepselectdata_e.htm
- IPCC (2007) *Climate Change 2007: The Physical Science Basis*, Cambridge University Press, Cambridge, U.K. and NY, U.S.A., 996 pp.
- Ishida H *et al.* (2009) Possibility of recent changes in vertical distribution and size composition of chlorophyll-a in the western North Pacific region. *J. Oceanogr.* **65**: 179–186.
- JMA (2001) Data Report of Oceanographic Observation, vol. S1, pp. 84–92, CD-ROM.
- Jo CO *et al.* (2007) Asian dust initiated early spring bloom in the northern East/Japan Sea. *Geophys. Res. Lett.* **34**: L05602, doi:10.1029/2006GL027395.
- JODC (2004) Joint Global Ocean Flux Study North Pacific Process Study Data Set, CD-ROM.
- KANSO (2006) KANSO Data Library, <http://www.kanso.co.jp/ocean/html-doc/japanese/west-cosmic/top3.html>
- Karl DM *et al.* (2001) Long-term changes in plankton community structure and productivity in the North Pacific Subtropical Gyre: the domain shift hypothesis. *Deep-Sea Res. II* **48**: 1449–1470, doi:10.1016/S0967-0645(1400)00149-00141.
- Kettle AJ *et al.* (1999) A global database of sea surface dimethylsulfide (DMS) measurements and a procedure to predict sea surface DMS as a function of latitude, longitude, and month. *Global Biogeochem. Cycles* **13**: 399–444, doi:10.1029/1999GB900004.
- Knap A *et al.* (1996) Protocols for the Joint Global Ocean Flux Study (JGOFS) core measurements, vi+170 pp. Reprint of the IOC Manuals and guides No. 29, UNESCO 1994.

- Levitus S *et al.* (2000) Warming of the world ocean. *Science* **287**: 2225–2229.
- Levitus S *et al.* (2001) Anthropogenic warming of Earth's climate system. *Science* **292**: 267–270, doi:10.1126/science.1058154.
- Mahowald NM *et al.* (2005) Atmospheric global dust cycle and iron inputs to the ocean. *Global Biogeochem. Cycles* **19**: GB4025, doi:10.1029/2004GB002402.
- Maldonado MT *et al.* (2001) Iron uptake and physiological response of phytoplankton during a mesoscale Southern Ocean iron enrichment. *Limnol. Oceanogr.* **46**: 1802–1808.
- Malin G, Kirst GO (1997) Algal production of dimethyl sulfide and its atmospheric role. *J. Phycol.* **33**: 889–896.
- NCEP/NCAR (2006) The NCEP/NCAR Reanalysis Project at the NOAA-CIRES Climate Diagnostics Center, <http://www.cdc.noaa.gov/cdc/reanalysis/>
- Nishioka J *et al.* (2007) Iron supply to the western subarctic Pacific: importance of iron export from the Sea of Okhotsk. *J. Geophys. Res.* **112**: C10012, doi:10.1029/2006JC004055.
- NOAA (2006) NOAA/PMEL DMS Data Server, <http://saga.pmel.noaa.gov/dms/>
- Ohshima KI, Martin S (2004) Introduction to special section: Oceanography of the Okhotsk Sea. *J. Geophys. Res.* **109**: C09S01, doi:10.1029/2004JC002604.
- Ohshima KI *et al.* (2006) Interannual variability of sea ice area in the Sea of Okhotsk: importance of surface heat flux in fall. *J. Meteorol. Sci. Jpn.* **84**(5): 907–919.
- Ohtani K (1991) To confirm again the characteristics of the Oyashio. *Bull. Hokkaido Natl. Fish. Res. Inst.* **55**: 1–24.
- Ono T *et al.* (1998) Distribution of total carbonate and related properties in the North Pacific along 30N. *J. Geophys. Res.* **103**: 30873–30883.
- Ono T *et al.* (2001) Temporal increase of phosphate and apparent oxygen utilization in the subsurface waters of western subarctic Pacific from 1968 and 1998. *Geophys. Res. Lett.* **28**: 3285–3288.
- Orr JC *et al.* (2005) Anthropogenic ocean acidification over the twenty-first century and its impact on calcifying organisms. *Nature* **437**: 681–686, doi:10.1038/nature04095.
- Osafune S, Yasuda I (2006) Bidecadal variability in the intermediate waters of the northwestern subarctic Pacific and the Okhotsk Sea in relation to 18.6-year period nodal tidal cycle. *J. Geophys. Res.* **111**: C05007, doi:10.1029/2005JC003277.
- Price NM (2005) The elemental stoichiometry and composition of an iron-limited diatom. *Limnol. Oceanogr.* **50**(4): 1159–1171.
- Raymond PA, Cole JJ (2003) Increase in the export of alkalinity from North America's largest river. *Science* **301**: 88–91, doi:10.1126/science.1083788.
- Sabine CL *et al.* (2004) Temporal evolution of the North Pacific CO₂ uptake rate. *J. Oceanogr.* **60**: 5–15.
- Saltzman ES *et al.* (1993) Experimental determination of the diffusion coefficient of demethylsulfide in water. *J. Geophys. Res.* **98**: 16481–16486, doi:10.1029/93JC01858.
- Sarma VVSS *et al.* (2002) Increase of total alkalinity due to shoaling of aragonite saturation horizon in the Pacific and Indian Oceans: Influence of anthropogenic carbon inputs. *Geophys. Res. Lett.* **29**: 1971, doi:10.1029/2002GL015135.
- Sarmiento JL *et al.* (2004) High-latitude controls of thermocline nutrients and low latitude biological productivity. *Nature* **427**: 56–60, doi:10.1038/nature02127.
- Simó R, Dachs J (2002) Global ocean emission of dimethylsulfide predicted from biogeophysical data. *Global Biogeochem. Cycles* **16**: 1078, doi:10.1029/2001GB001829.
- Stephens C *et al.* (2002) World Ocean Atlas 2001, Volume 1: Temperature. In *NOAA Atlas NESDIS 49* (ed. Levitus S), U.S. Government Printing Office, Washington, D.C., 167 pp., CD-ROMs.
- Strickland JDH, Parsons TR (1968) A practical handbook of seawater analysis. *Fish. Res. Board of Canada, Bull.* **167**: 65–75.
- Suzuki K *et al.* (2002) East-west gradients in the photosynthetic potential of phytoplankton and iron concentration in subsurface Pacific Ocean during early summer. *Limnol. Oceanogr.* **47**: 1581–1594.
- Takahashi T *et al.* (2002) Global sea-air CO₂ flux based on climatological surface ocean pCO₂, and seasonal biological and temperature effects. *Deep-Sea Res. II* **49**: 1601–1622, doi:10.1016/S0967-0645(02)00003-6.
- Thomas H *et al.* (2007) Rapid decline of the CO₂ buffering capacity in the North Sea and implications for the North Atlantic Ocean. *Global Biogeochem. Cycles* **21**: GB4001, doi:10.1029/2006GB002825.
- Tsurushima N *et al.* (2002) Seasonal variations of carbon dioxide system and nutrients in the surface mixed layer at station KNOT (44°N, 155°E) in the subarctic western North Pacific. *Deep-Sea Res. II*

- 49: 5377–5394.
- Ueno H, Yasuda I (2003) Intermediate water circulation in the North Pacific subarctic and northern subtropical regions. *J. Geophys. Res.* **108**: 3348, doi:3310.1029/2002JC001372.
- Wakita M *et al.* (2003) Oceanic uptake rate of anthropogenic CO₂ in a subpolar marginal sea: The Sea of Okhotsk. *Geophys. Res. Lett.* **30**(24): 2252, doi:10.1029/2003GL018057.
- Wanninkhof R, McGillis WR (1999) A cubic relationship between air-sea CO₂ exchange and wind speed. *Geophys. Res. Lett.* **26**: 1889–1892, doi:10.1029/1999GL900363.
- Watanabe S *et al.* (1995a) Relation between the concentrations of DMS in surface seawater and air in the temperate North Pacific region. *J. Atmos. Chem.* **22**: 271–283, doi:10.1007/BF00696638.
- Watanabe S *et al.* (1995b) Dimethyl sulfide widely varying in surface water of the eastern North Pacific. *Mar. Chem.* **51**: 253–259.
- Watanabe YW, Nishioka J (2007) Preliminary report of kh06 cruise of R/V Khromov. *Amur-Okhotsk Project, Research Institute for Humanity and Nature.*
- Watanabe YW *et al.* (1994) Chlorofluorocarbons in the central North Pacific and southward spreading time of North Pacific Intermediate Water. *J. Geophys. Res.* **99**: 25195–25213.
- Watanabe YW *et al.* (1995) Dilution of North Pacific Intermediate Water studied with chlorofluorocarbons. *J. Oceanogr.* **51**: 133–144.
- Watanabe YW *et al.* (2001) Probability of a reduction in the formation rate of the subsurface water in the North Pacific during the 1980s and 1990s. *Geophys. Res. Lett.* **28**(17): 3289–3292, doi:10.1029/2001GL013212.
- Watanabe YW *et al.* (2003) Synchronous bidecadal periodic changes of oxygen, phosphate and temperature between the Japan Sea deep water and the North Pacific intermediate water. *Geophys. Res. Lett.* **30**(24): 2273, doi:10.1029/2003GL018338.
- Watanabe YW *et al.* (2005) Spatiotemporal decreases of nutrients and chlorophyll-a in the surface mixed layer of the western North Pacific from 1971 to 2000. *J. Oceanogr.* **61**: 1011–1016.
- Watts SF (2000) The mass budgets of carbonyl sulfide, dimethyl sulfide, carbon, disulfide, and hydrogen sulfide. *Atmos. Environ.* **34**: 761–779.
- Whitney FA *et al.* (2007) Persistently decreasing oxygen levels in the interior waters of the eastern subarctic Pacific. *Prog. Oceanogr.* **75**: 179–199.
- Wilks DS (1995) *Statistical Methods in the Atmospheric Sciences*. Academic Press, New York.
- Wong CS *et al.* (2002) Seasonal changes in the distribution of dissolved organic nitrogen in coastal and open-ocean waters in the North East Pacific; sources and sinks. *Deep-Sea Res. II* **49**: 5759–5773.
- Wong CS *et al.* (2005) Temporal and spatial distribution of dimethylsulfide in the subarctic northeast Pacific Ocean: a high-nutrient-low chlorophyll region. *Tellus B* **57**: 317–331.
- Yamagishi H *et al.* (2005) Contributions of denitrification and mixing on the distribution of nitrous oxide in the North Pacific. *Geophys. Res. Lett.* **32**: L04603, doi:04610.01029/02004GL021458.
- Yamamoto-Kawai M *et al.* (2004) Chlorofluorocarbons in the Sea of Okhotsk: Ventilation of the intermediate water. *J. Geophys. Res.* **109**: C09S11, doi:10.1029/2003JC001919.
- Yasuda I *et al.* (2006) Possible explanation linking 18.6-year period nodal tidal cycle with bi-decadal variations of ocean and climate in the North Pacific. *Geophys. Res. Lett.* **33**: L08606, doi:10.1029/2005GL025237.
- Yentsch CS, Menzel DW (1963) A method for the determination of phytoplankton chlorophyll and phaeophytin by fluorescence. *Deep-Sea Res.* **10**: 221–231.
- Yoshikawa C *et al.* (2006) Distribution of N* in the Sea of Okhotsk and its use as a biogeochemical tracer of the Okhotsk Sea Intermediate Water formation process. *J. Mar. Syst.* **63**: 49–62.